Title

Modeling the Effects of Dimerization and Bulk Diffusion on the Evaporative Behavior of Secondary Organic Aerosol Formed from α-Pinene and 1,3,5-Trimethylbenzene

Journal

ACS Earth and Space Chemistry, 4(11)

ISSN

2472-3452

Authors

Morino, Yu
Sato, Kei
Jathar, Shantanu H
et al.

Publication Date

2020-11-19

DOI

10.1021/acsearthspacechem.0c00106

Peer reviewed

Modelling the Effects of Dimerization and Bulk Diffusion on the Evaporative Behavior of Secondary Organic Aerosol Formed from α-Pinene and 1,3,5-Trimethylbenzene

Yu Morino,[*,†] *Kei Sato,*[†] *Shantanu H. Jathar,*[‡] *Kiyoshi Tanabe,*[†] *Satoshi Inomata,*[†] *Yuji Fujitani,*[†] *Sathiyamurthi Ramasamy,*[†] *and Christopher D. Cappa*[§]

[†]National Institute for Environmental Studies, Tsukuba, Ibaraki, 305-8506, Japan

[‡]Department of Mechanical Engineering, Colorado State University, Fort Collins, CO, 80523, USA

[§]Department of Civil and Environmental Engineering, University of California, Davis, CA, 95616, USA

ABSTRACT: Volatility determines the gas-particle partitioning of organic compounds. Volatility is thus a key property needed to understand the behavior of organic aerosol (OA) in the atmosphere. Various studies have been conducted to experimentally measure and numerically simulate distributions of OA volatility. The observed OA evaporation rates have generally been slower than the rates assuming instantaneous gas-particle equilibrium and volatility estimated from secondary organic aerosol (SOA) formation experiments. Particle phase diffusion and/or low volatility compounds, such as oligomers and highly oxygenated molecules, could limit the evaporation of OA, though the relative contributions of these factors are still uncertain. In this study, we conducted model simulations using a volatility basis set framework with consideration of kinetic gas-particle partitioning, formation and dissociation of dimers, and particle-phase diffusion to reproduce observed evaporative behaviors of SOA formed from α-pinene ozonolysis and 1,3,5-trimethylbenzene (TMB)/NO_x photooxidation. Based on simulations constrained by various volatility distributions derived from chemical analysis or heating experiments, we found that both dimerization and slow particle-phase diffusion contributed to the observed slow evaporation under dry conditions. In contrast, particle-phase diffusion did not practically inhibit SOA evaporation under humid conditions. The similarity of the fitted parameters, including dimer formation/dissociation rates and bulk diffusivity, for SOA from α-pinene and 1,3,5-TMB under dry conditions suggested that these processes are important for both monoterpene and aromatic SOA. Evaporation rates of SOA from α-pinene in this study were slower than the rates reported in previous experimental studies. This difference could be partly explained by differences in the experimental setups, including the treatment of organic vapors.

KEYWORDS: secondary organic aerosol, dilution-induced evaporation, dimer formation, bulk diffusion, kinetic model, aerosol particle viscosity, vapor wall loss.

1. Introduction

Organic aerosol (OA) represents a large fraction (20–90%) of submicron aerosol,[1] and thus, understanding the behavior and sources of OA is necessary. For accurate representation of OA by numerical simulation models, we need to understand both chemical and physical properties of OA. For chemical properties, there is a large diversity in the composition of OA but not all constituents of OA have been identified.[2, 3] Although there are several approaches to explicitly simulate OA composition,[4-7] the computational burden of these explicit simulations is large and OA is represented by grouping or lumping compounds. To simulate secondary organic aerosol (SOA), a wide variety of organic compounds have been classified based on their physicochemical properties, such as volatility (or vapor pressure), oxidation state, carbon number, or number of functional groups.[8-11] In addition to semi-volatile organic compounds (SVOC), highly oxygenated organic molecules (HOMs)[12-14] and oligomers,[15, 16] both of which can be extremely low volatility or low volatility organic compounds (ELVOC or LVOC, respectively), make significant contributions to SOA. The formation of these compounds has thus been introduced in some SOA models.[17-20] Physical properties, particularly volatility and bulk diffusion coefficients, are also important in accurately representing OA, because these processes strongly influence the gas/particle partitioning process. In many chemical transport models, rapid equilibrium between the gas and particulate-phases is assumed for organic compounds,[21, 22] though studies during the last decade have suggested that this assumption may not hold for all conditions and systems. For example, evaporation of laboratory-generated or ambient SOA after dilution or scavenging of vapors are associated with a timescale longer than several hours.[23, 24] Trump and Donahue [17] and Kolesar, et al. [18] have indicated that oligomer formation and its slow dissociation could be one explanation for the slow evaporation of SOA, while Yli-Juuti, et al. [25] have shown that particulate-phase diffusion

62 is a limiting factor of slow evaporation under dry conditions. In contrast, Saleh, et al. [26] and Saha
63 and Grieshop [27] have indicated that the timescale for gas-particle equilibrium is less than 1 h and
64 that the equilibrium assumption can be applied in chemical transport models given typical model
65 timesteps. Applicability of the equilibrium assumption is an undecided issue, and there is presently
66 no consensus about its use.

67 Understanding of both physical and chemical properties is necessary to reveal the factors that
68 control SOA evaporation. It has been pointed out that the SOA volatility distribution estimated
69 from formation experiments using a traditional volatility basis set (VBS) framework includes more
70 volatile components than that estimated from dilution experiments, heating experiments, or
71 chemical analysis combined with parameterization techniques[27-30]. This suggests that the presence
72 of low-volatility compounds or kinetic inhibition affects SOA evaporation processes. To our
73 knowledge, few previous modeling studies have considered both dimerization and bulk diffusion
74 [20, 31], and the constraints needed to determine the controlling factors of SOA evaporation are still
75 lacking. Recently, the C^* distribution of α-pinene SOA has been evaluated from chemical analyses
76 [32, 33] and heating experiments [27, 34], and these data could potentially be used as constraints for the
77 estimation of the model parameters that determine SOA evaporation. For the simulation of bulk
78 diffusion in viscous particles, Shiraiwa, et al. [35] and DeRieux, et al. [36] have developed a
79 parameterization process for estimation of the glass transition temperature (T_g) of individual SOA
80 compounds. Using their parameterization process, bulk diffusivity can be calculated from the
81 chemical composition of SOA. However, the consistency of this parameterization process for
82 predicting SOA evaporation is a concern and should be evaluated using independent estimates.

83 In addition, Sato, et al. [37] conducted dilution and heating experiments in which they measured
84 the evaporative behaviors and chemical composition of SOA from 1,3,5-trimethylbenzene

(TMB).[37] Most research on the evaporative behavior of SOA has concerned the SOA from biogenic volatile organic compounds (VOC). However, SOA from anthropogenic VOC can make important contributions to atmospheric OA in urban regions,[38, 39] and the evaporative behavior of anthropogenic SOA should therefore be understood as well. SOA mass yields and SOA properties (volatility and O:C ratios) differ between anthropogenic and biogenic SOA, and experiments with anthropogenic SOA should therefore enhance understanding of the behavior of ambient SOA.

In this study, we conducted model simulations that took into consideration kinetic gas-particle partitioning, formation and dissociation of dimers, and particle-phase diffusion, and we assessed the effects of these processes on the evaporative behavior of SOA. We first conducted simulations with single-component SOA to evaluate the sensitivity of its evaporative behavior to model parameters related to volatility, dimer formation/dissociation, and particle-phase diffusion. We then conducted simulations for multi-component SOA in which estimates of dimer formation/dissociation rates and bulk diffusivity were constrained by SOA concentrations observed during the formation and dilution experiments and by the volatility distributions estimated from previous chemical analyses or heating experiments. Finally, we compared the simulated evaporative behavior and estimated model parameters between monoterpene and aromatic SOA. Based on these analyses, we assessed the influence of dimerization and bulk diffusion processes on the formation and evaporation of SOA.

2. Methods

2.1. Chamber Experiments of SOA Formation and Dilution

Our modeling relies on chamber experiments performed by Sato, et al. [33, 37]. Sato, et al. [33, 37] conducted twelve experiments using SOA from α-pinene ozonolysis and seven using SOA from

1,3,5-TMB/NO_x photooxidation to estimate SOA volatility distributions. We conducted box model simulations for ten of these previous experiments (Table 1), in which SOA behavior after isothermal dilution was measured. Because the experimental setup for α-pinene ozonolysis and 1,3,5-TMB photooxidation have been described in Sato, et al. [33] and Sato, et al. [37], respectively, we provide only a brief description of those experiments here. A 6-m^3 Teflon-coated stainless-steel chamber was used for the experiments under dry conditions (relative humidity (RH) < 1%), and a 6-m^3 fluorinated ethylene polyethylene (FEP) film bag (1.81 × 1.81 × 1.81 m^3, 50-μm film thickness) was used for experiments under humid conditions (RH = 40%). A comparison of the background concentrations of particulate matter and VOC in the chamber and film bag is shown in Table S2 of the Supporting Information (SI). Considering these background concentrations and the maximum SOA yields[21], the contribution of these background concentrations to the produced SOA was about 0.03% in the chamber used for the dry experiments and about 0.3% in the film bag used for the humid experiments. Thus, we considered the contributions of the background to be negligible in our analysis. The requisite amounts of precursors (i.e., α-pinene and 1,3,5-TMB), ozone, or other gaseous compounds were injected into these chambers (Table 1). Particle size distributions were measured with a scanning mobility particle sizer (SMPS) (Model 3034, TSI Inc., USA). The effective particle density of the SOA from α-pinene ozonolysis was estimated to be 1.34 g cm^{-3} by using a custom-made differential mobility analyzer and aerosol particle mass analyzer (APM) (Model 3600, Kanomax Inc., Japan).

Offline chemical analysis was performed using a positive electrospray ionization-liquid chromatograph/time-of-flight-mass spectrometer (LC-TOF-MS, Agilent Technologies, UK). In each experiment, an aerosol sample for LC-TOF-MS analysis was collected on a Teflon filter (Sumitomo Electric Industries, Japan, 47 mm φ, pore size 1 μm) at a rate of 16.7 L min^{-1} for 30

min after the reaction finished. Sato, et al. [33, 37] have estimated volatility distributions of SOA from the concentrations and molecular formulas of the organic species identified through LC-TOF-MS analysis. Various parameterizations were used to relate the molecular formulas to the saturation concentrations (C^*). In one method, for the SOA from both α-pinene and 1,3,5-TMB, the C^* distribution was estimated with a two-dimensional function (C^* was parameterized as a function of the number of carbon and oxygen atoms, 2-D method).[28] To assess the uncertainty, Sato, et al. [33] used a one-dimensional function (C^* was parameterized as a function of molecular weight (MW))[29] with a binary fit for products of α-pinene ozonolysis with low MW ($m/z < 300$) and high MW ($m/z \geq 300$) (binary method). Sato, et al. [37] also used the two-dimensional function to fit to $\log_{10}(C^*)$ data calculated by the SPARC (SPARC Performs Automated Reasoning in Chemistry) calculator[40] for products from TMB photooxidation (SPARC method). Sato, et al. [33, 37] have shown that only a small portion of HOMs decompose and that the root mean square error (RMSE) and mean bias of the $\log_{10}(C^*)$ estimated by SPARC and the two-dimensional function parameterized in accord with Sato, et al. [37] are 1.9 and 0.0, respectively. The RMSE and mean bias between the $\log_{10}(C^*)$ estimated by the SPARC and the original parameterization of the two-dimensional function[28] were 2.2 and –0.4, respectively. Quantitative analysis of the uncertainty of the estimated C^* distribution is difficult because the mass identified by the LC-MS analysis could only explain at most only 30% of the total SOA mass,[3] however, these values still provide a measure of the uncertainty.

Evaporative behaviors associated with isothermal dilution were measured by injecting air from the reaction chamber into a clean 6 m^3 FEP film bag (external dilution chamber, EDC) using a dilution ejector (FPS-4000, Dekati Ltd., Finland). The clean dilution air used was from a clean-air generator (Model 1160, Thermo Fisher Scientific, USA) for dry experiments (RH < 1%) and from

a purified air generator (DAR-2000, Horiba Stec Ltd., Japan) for humid experiments (RH = 40%). The dilution ratios were 20–77 (α-pinene) and 20–86 (TMB). The temperature of the laboratory was controlled at 298 ± 1 K. The particle size distribution, particle density, and CO concentration in the EDC were monitored after dilution of the SOA, and the CO concentration was used to estimate the dilution ratio. It has been shown by McFiggans, et al. [41] that the composition of SOA from α-pinene photooxidation was changed by the addition of CO. However, Sato, et al. [33] have shown that the composition of SOA from α-pinene ozonolysis did not markedly change even with addition of a large amount of CO (0.83 torr = 1092 ppmv). In the dilution experiments of Sato, et al. [33], CO was added as a dilution tracer at a much lower concentration (~ 20 ppmv), and therefore we consider that the added CO did not greatly change the composition of the SOA products.

2.2. Framework of Organic Aerosol Model

For the modeling analyses of SOA formation and evaporation after isothermal dilution, we used a one-dimensional volatility basis set (1D-VBS) framework[9] that accounted for formation and dissociation of dimers[17, 18] and kinetic limitations to diffusion inside the particle-phase.[19] Products of VOC oxidation (i.e., α-pinene + ozone or 1,3,5-TMB/NO_x + light) were represented as five surrogate compounds with saturation concentration (C_i^*) of 0.1, 1, 10, 100, and 1000 μg m^{-3}. The mass yield of compound *i* was represented by a_i. We should note that compounds with a C^* of 0.1 μg m^{-3} were practically non-volatile under our experimental conditions. We therefore did not consider monomeric compounds with a C^* <0.1 μg m^{-3} in this study. The formulation of the C^* distribution is explained in Section 3.2.

For the calculation of kinetic gas-particle partitioning, we adopted the equations formulated by Zaveri, et al. [19] These equations were used to calculate condensation/evaporation rates of organic

compounds while taking into consideration volatility, gas-phase diffusion, interfacial mass accommodation, particle-phase diffusion, and particle-phase reactions (oligomerization in this study). Section S1 of the SI provides details of these equations. We did not calculate coagulation, given that mean volume diameter was larger than 150 nm immediately after the start of the formation experiments (Figure S1 of the SI) and contribution of coagulation on the size distribution is small.

An accommodation coefficient (α) and particle-phase diffusivity (D_b) were uncertain parameters in these simulations. Recent work has found that the mass accommodation coefficient for both laboratory and field aerosols is close to or equal to 1.[42] Without an explicit treatment of the bulk diffusion coefficient, it is likely that the mass transfer limitations observed in earlier work may have been attributed to a low value of the mass accommodation coefficient (≤0.1).[26, 27] As the bulk diffusion coefficient is explicitly modeled in this work, we assumed the mass accommodation coefficient to be equal to 1 for all our simulations.

The basic formulations of dimer formation and dissociation reactions were based on the formulations of Trump and Donahue [17] and Kolesar, et al. [18]. We simulated reversible, condensed-phase reactions with dimer formation and dissociation rates as $R_f = k_f {w_m}^2, R_r = k_r w_d$, respectively, where w_m and w_d represent the mass fractions of monomer and dimer in the particle phase, and k_f (s^{-1}) and k_r (s^{-1}) are the formation and dissociation rate constants, respectively, for dimers. Formation and dissociation rates of dimers should differ among dimer types, such as hemiacetals, acetals, esters, and ethers.[43, 44] However, these differences were not considered in this study because the differences in k_f and k_r among dimer types are not sufficiently constrained to warrant separate treatment in the simulation. We therefore used average k_f and k_r values in this study. We assumed that dimers are non-volatile in our simulations because the C^* values of dimers

200 are less than 1 μg m^{-3}. In addition, we assumed that only homodimers (dimers formed from
201 monomers with the same C^*) are formed, as in Kolesar, et al. [18], and that k_f and k_r are the same for
202 all C^* species. Such simplification might not be realistic as already discussed in Trump and
203 Donahue [17] and Kolesar, et al. [18]. However, for the parameter estimation from the experimental
204 data, number of model parameters should be reduced, so that we applied such simple module.
205 For the simulations with single C^* SOA (Section 3.2.1), size distributions were tracked using a
206 sectional approach with 60 sections of particle diameters ranging from 10 to 1000 nm. Initial size
207 distributions were based on observational data, and particle growth due to condensation or
208 shrinkage by evaporation was considered. We assumed log-normal distributions of particle sizes
209 for the simulations with multi-component SOA (Section 3.2.2) during both the formation and
210 dilution experiments, because the observed size distributions were reasonably mono-modal as
211 shown in Section 3.1.
212
213 2.3. Model simulation of chamber experiments
214 As noted in Section 2.1, we conducted simulations for experiments of both SOA formation and
215 dilution (Table 1). The particle wall loss (PWL) rate in the SOA reaction chamber was calculated
216 from experimental data. For the α-pinene ozonolysis experiments, after the α-pinene had reacted
217 away the change in the geometric mean diameter was small (–3 nm/hr), whereas the SOA mass
218 concentrations decreased at a rate of 0.128 h^{-1} because of particle deposition to the walls and the
219 small amount of dilution associated with instrument sampling. In the case of the SOA produced
220 by photooxidation of TMB, SOA-forming chemical reactions between SVOC and OH could
221 continue beyond the point at which all the TMB had reacted, and we were thus unable to estimate
222 the PWL rate of TMB-SOA directly from our experimental data. Instead, we assumed a PWL rate

of 0.22 h^{-1}, which is the PWL rate reported for ammonium sulfate particles in the same diameter range.[37] PWL rates in the ejector were calculated from the changes of the size distribution and mass concentration of the SOA. The geometric mean volume diameter of the SOA before and just after passage through the ejector changed by 0.2–2% under dry conditions and by 4–7% under humid conditions. Previous experiments have shown that the PWL rate in the ejector does not depend strongly on the distribution of particle diameters around the peak diameter.[45] Based on this assumption, we estimated the evaporation rate of SOA in the ejector from the change of the geometric mean volume diameter. Thus, the fraction of SOA evaporated during passage through the ejector was $[1 - (d_{vm}(\text{after ejector})/d_{vm}(\text{before ejector}))^3]$. Then, a further decrease of the SOA mass was caused by size-independent PWL. In other words, the fraction of particles deposited on the ejector wall to particles introduced into the ejector was assumed to equal $[1 - \frac{C^*_{SOA}(\text{after ejector})/C^*_{SOA}(\text{before ejector})}{(d_{vm}(\text{after ejector})/d_{vm}(\text{before ejector}))^3}]$, where C^*_{SOA} is the mass concentration of the SOA (corrected by the dilution ratio), and d_{vm} is the volume-mean diameter. We compared the measured and calculated volume fraction remaining (VFR) from the equation $\text{VFR(t)} = \left(\frac{d_{vm}(\text{t})}{d_{vm}(\text{before ejector})}\right)^3$ for the analysis of the SOA evaporation rate; in this way uncertainties associated with the PWL in the EDC were minimized. The volatility dependent vapor wall loss (VWL) in both the reaction chamber and the EDC were calculated by applying the formulation of Krechmer, et al. [46] Details are provided in Section S2 of the SI.

As shown in Sections 3.2.2 and 3.2.3, we estimated plausible sets of parameters by fitting the model to observational data. Parameter estimation was conducted by using a nonlinear programming solver, the Nelder-Mead simplex algorithm[47] of MATLAB (R2018a, The MathWorks, Inc., MA, USA).

3. Results and Discussion

3.1. Experimental Results

We first compared the observed time-dependent VFR from α-pinene[33] and 1,3,5-TMB[37] with the rates reported in other studies (Figure 1). Details of the experimental setups of the other studies are provided in the cited publications, and we briefly introduce the methodologies used in Table S3 of the SI. In Sato, et al. [33, 37], the time-dependent VFR of the SOA from α-pinene and 1,3,5-TMB were similar functions of time under dry conditions: the VFR of the SOA decreased by 14–20% within 1 h after dilution, and there was continued slow evaporation even after 2–3 h. Evaporation was slightly faster for the dry SOA from α-pinene versus the SOA from 1,3,5-TMB. To our knowledge, no studies other than Sato, et al. [37] measured evaporative behaviors of aromatic SOA by the isothermal dilution method, though this result was consistent with other heating experiments,[48, 49] which have shown that dry SOA from aromatic VOC is less volatile than the SOA from monoterpenes. Of course, factors other than precursors, including oxidants,[48, 50, 51] SOA concentrations,[48] or reaction timescales[52, 53] should also be important factors controlling SOA volatility. Therefore, we cannot conclude that anthropogenic SOA is more (or less) volatile than biogenic SOA.

The evaporation rate of SOA from α-pinene was significantly higher under humid conditions (RH = 40%) versus dry conditions. The VFR decreased by about 35% in 1 h after dilution and continued decreasing even after 3 h. This RH dependence is consistent with previous studies,[24, 25, 54] who have measured isothermal SOA evaporation rates at different RH. By contrast, D'Ambro, et al. [55] have shown that the evaporation rates of SOA from α-pinene ozonolysis did not indicate RH dependence within a range of 20%–80% RH. It should be noted that D'Ambro, et al. [55] measured evaporation rates of SOA on filters, whereas evaporation rates of suspended SOA were

measured in other studies. In addition, the lowest RH in the experiments of D'Ambro, et al. [55] was 20%, which is higher than the RH in other dry experiments, and this difference could explain the different evaporation rates.[54] Consideration of these differences between D'Ambro, et al. [55] and other studies may account for the apparently different behavior of the SOA evaporation in these studies. Another difference in the humid experiments is the RH during SOA formation. SOA produced under dry conditions was exposed to different RH by Yli-Juuti, et al. [25] and D'Ambro, et al. [55], whereas SOA were formed under humid conditions (RH = 40%) in the humid experiments performed by Sato, et al. [33, 37]. However, the SOA evaporation rate was not affected by the RH (dry or 30%) during SOA formation in the experiments conducted by Yli-Juuti, et al. [25]. Overall, because the experimental setups of the individual studies differed, there were differences in the evaporative behaviors of SOA from α-pinene under both dry and humid conditions (Figure 1). In some previous studies, evaporation was accelerated because semi-volatile vapors were removed artificially[23, 55] or they were likely removed within a short time in a stainless steel chamber.[25] However, semi-volatile vapors were not intentionally removed in other chamber experiments.[33, 37, 56] In addition, concentrations, diameters, and the conditions of particles (e.g., on filters in D'Ambro, et al. [55]) differed between experiments. The implications of these differences are discussed in Section 3.2.3. We used our experimental data for the modeling analysis presented in Section 3.2 and Section 3.3. We should note that during both the dry and humid experiments, evaporation still occurred, even several hours after the start of dilution. This behavior is consistent with the findings from other previous experiments (Figure 1). It is reasonable that evaporation still occurs in an open system (with continuous removal of vapors), even at several hours after the perturbation. In a closed system (with a finite amount of vapor, chamber experiments in this case), not only kinetic limitation, but also VWL would contribute to this continuous decrease of VFR.

The derived C^* distributions of total (gas + particle) organic compounds [33, 37] were also compared with those reported in the literature (Figure 2). We found that the fraction of total gas and particulate-phase oxidation products ($f_i = a_i/\Sigma(a_i)$) of C^* were in the range of 10^{-9} – 10^{3} μg m^{-3}. A brief summary of the derivations in the previous studies is given in Table 2 and Section S3 of the SI. Even though our estimate includes uncertainties (Section 2.1), the derived C^* distributions of total (gas + particle) organic compounds [33, 37] based on the measured particle composition of the SOA from α-pinene and 1,3,5-TMB showed similar trends: the low-volatility (mostly dimers[33]) and semi-volatile (C^* = 10–1000 μg m^{-3}) organic compounds made marked contributions after completion of the reaction in the reaction chamber (Figure 2). In these cases, the dimer fractions (f_{dimer} = [dimer]/[SOA]) calculated using data from the LC-TOF-MS analysis were similar for both SOA types, 0.59 for the SOA from α-pinene and 0.58 for the SOA from 1,3,5-TMB. Previous experimental studies have also indicated the important contributions of oligomers, but their contributions significantly varied from a few percent to ~70% among studies[2, 16, 33, 37, 57, 58]. The f_{dimer} estimated by Sato, et al. [33, 37] is within a range of these previous estimates. The C^* distributions shown in Figure 2 were derived from chemical analysis [34] or heating experiments [27, 32, 33]. We should note that these estimates do not include the contributions of dimers to the distributions. Isaacman-VanWertz, et al. [34] measured concentrations of gaseous compounds and estimated aerosol contributions from their vapor pressures. Thus, it is presumed that the contributions of LVOC and dimers were not properly calculated. In heating measurements, the oligomers could evaporate or decompose, so understanding of the heat-induced evaporative behaviors of oligomers is complicated [17, 59]. Considering this uncertainty, the contributions of dimers might not be accurately estimated from heating experiments. However, even with these limitations, all the estimates showed that SVOC made important contributions to the distributions (*fi* of compounds

with C^* = 100–1000 μg m^{-3} was 0.36–0.69). For the practical model simulation, C^* distributions should be determined from the limited, currently available datasets, and thus, the C^* distributions and f_{dimer} values were used as constraints in the simulations, and the implications of the contributions of SVOC are discussed in Section 3.2.2.

The evolution of particle size during the formation and dilution experiments is shown in Figure S1. Size distributions during both experiments were reasonably unimodal and were well fit to log-normal functions throughout the experiments (geometric mean volume diameter around 200–400 nm). Therefore, we assumed log-normal distributions for the simulation of the multi-component SOA.

3.2. Sensitivity Simulations for SOA from α-Pinene

3.2.1. Simulations for single-component SOA

We simulated the evaporation behavior of SOA in the EDC assuming that the SOA was composed of compounds with the same C^* value, but with other parameters allowed to vary, for the two objectives. First, this allowed for assessment of the sensitivity of simulated SOA concentrations obtained from dilution experiments to the assumed saturation concentration C^*, the monomer-dimer conversion rates (dimer formation rate k_f and dissociation rate k_r), and the bulk diffusivity D_b (Figure 3). Second, the simulation models often need to be simplified because of limitations of computational resources, and therefore simulation results with a simpler framework provide information that is useful for practical application. Here, we focus on understanding the influence of RH and thus consider only SOA from α-pinene ozonolysis. As already noted, gas-particle equilibrium was not attained during the experiments under both dry and humid conditions. However, under dry conditions, evaporation rates slowed even on a logarithmic timescale during

the experiments of this study and those of Grieshop, et al. [56] In contrast, the evaporation rates did not slow on a logarithmic timescale during experiments conducted by other groups.[23, 25, 55] This point is also discussed in Section 3.2.3.

It was apparent from simulations without consideration of dimer formation (k_f = 0) and bulk diffusion that time-dependent VFR was particularly sensitive to C^* (Figure 3). To quantitatively evaluate the model performance, the RMSE of measured and simulated VFR during the dilution experiments was calculated in each case. In this study, derivation of logarithm of time t (i.e., 1/t) was used for weighting to reproduce the initial evaporative behavior ($\mathrm{RMSE} = \sqrt{\frac{\sum(\mathrm{VFR_{model,i}} - \mathrm{VFR_{obs,i}})^2 / t_i}{\sum(1/t_i)}}$, where $\mathrm{VFR_{model,i}}$ and $\mathrm{VFR_{obs,i}}$ indicate simulated and observed VFR at time t_i). Here, the observed SOA concentrations after dilution were best reproduced in the cases with C^* =1.3–2.5 μg m^{-3} for experiments under dry conditions and 3.2–12.6 μg m^{-3} under humid conditions. However, the shapes of the evaporation curves were not well reproduced over the whole period for any single C^* for either RH. Nonetheless, these estimated C^* values were somewhat similar to an effective mass-weighted C^* (1–4 μg m^{-3}) estimated from observed evaporation rates of α-pinene ozonolysis SOA by D'Ambro, et al. [55] These C^* values are nonetheless greater than those estimated from chemical analysis (mass-weighted C^* was from 0.0017 μg m^{-3} [the binary method] to 0.25 μg m^{-3} [the 2-D method]).[33] This gap indicates that the evaporation and chemical properties of SOA cannot simply be represented by a single component calculation. In our experiments, OA concentrations decreased from ~10^3 μg m^{-3} in the reaction chamber to ~10^1 μg m^{-3} in the EDC.[33, 37] Because gas-particle partitioning at equilibrium is 1:1 for a compound with C^* identical to the OA concentration ($\frac{C_{gas,i}}{C_{aerosol,i}}$ for organic compound i is equal

to $\frac{C_i^*}{C_{OA}}$), it is reasonable that the mass loss resulted predominately from evaporation of compounds with C^* = 10–1000 μg m^{-3} (Figure 3).

Results of the sensitivity simulations to C^*, k_f (or f_{dimer}), k_r, D_b are summarized in Section S4 of the SI. For the parameter space considered here, the overall best results under the single C^* assumption were obtained when $D_b \geq 10^{-18}$ m^2 s^{-1}, f_{dimer} = 0.6, k_r = ~3 × 10^{-6} s^{-1}, and C^* = ~10 μg m^{-3} for dry experiments (Figures S2 and S3 of the SI). In the humid experiments (Figures S4 and S5 of the SI), generally similar results were obtained as in the dry experiments. However, there was a much clearer minimum in the RMSE that occurred at a comparably higher D_b (= 10^{-16} m^2 s^{-1}), lower f_{dimer} (= 0.4), and larger k_r (~3 × 10^{-5} s^{-1}). Also the simulation-observation agreement at low D_b ($\leq 10^{-18}$ m^2 s^{-1}) was notably worse for all combinations of the other parameters. We should note that SOA evaporation was not delayed in the simulations with $D_b \geq 10^{-16.5}$ m^2 s^{-1} for all the compounds, suggesting that SOA was not diffusion-limited in these simulations.

The changes of SOA sizes during dilution-induced evaporation are similar in scenarios with different k_f, k_r, and D_b values (Figure S6 of the SI). Namely, larger particles evaporated faster, and mean diameter decreased as evaporation proceeded. This particle-size evolution is consistent with the observed size changes. We therefore cannot constrain unique parameter sets of C^* distributions, k_f, k_r, and D_b from only SOA concentrations and size distributions during formation and dilution experiments.

Overall, the C^* and k_f (or f_{dimer}) determined the end-of-experiment concentrations, and sensitivities to these parameters were thus significant over the whole dilution experiment. In contrast, k_r and D_b determined equilibration timescales, and sensitivities to these parameters were thus apparent within the equilibration timescales calculated from these parameters. Dilution-induced evaporative behaviors have been shown to be highly sensitive to C^*, and we can thus

expect that this evaporative behaviors can be reproduced if we optimize the C^* distributions in multi-component systems, even with wide ranges of parameter values for k_f, k_r, and D_b[25]. In the next section, we constrained C^* distributions from chemical analysis data[33].

3.2.2. Simulations for multi-component SOA

(a) Without constraint of C^* distributions

The C^* distribution of VOC oxidation products (i.e., mass yield (a_i) of oxidation product with C_i^*) is one of the key factors that control the simulated SOA evaporation behavior, as discussed above. Here, we assess the ability of the model to reproduce the observed evaporation profiles where it is assumed that the compounds comprising the SOA have a distribution of C^* values (C^* = 0.1, 1, 10, 100, and 1000 μg m^{-3}). Simulations are performed for a variety of discrete k_f, k_r, and D_b combinations; for each pair of k_f and k_r, the D_b are varied over the range 10^{-19}–10^{-16} m^2 s^{-1}. The C^* distributions are determined by minimizing the difference between observed and simulated SOA concentrations in both the reaction chamber and the EDC. Here, an objective function for the above parameter optimization was the sum of RMSE of SOA concentrations in the reaction chamber (normalized by the observed SOA concentrations at the end of the formation experiments) and VFR in the EDC. Both are normalized parameters, so the weighting factors for RMSE for normalized SOA concentrations in the reaction chamber and VFR in the EDC were set equal. Simulations with this multiple-C^* system were conducted both for the reaction chamber and EDC. Thus, we explicitly calculated f_{dimer} after the formation experiment by inputting both k_f and k_r.

Figure 4 shows examples of fitting results for experiments under dry conditions. We find that, after optimization of the C^* distribution, any assumed combination of k_f and k_r used here allows for a reasonable match with the observed evaporation profile for the dry SOA when $D_b \geq 10^{-18}$ m^2 s^{-1}. For all cases, when $D_b = 10^{-19}$ m^2 s^{-1}, evaporation proceeds too slowly initially, leading to

overall marginal agreement with the observations even after optimization. The optimized C^* distributions obtained for the $D_b \geq 10^{-18}$ m^2 s^{-1} simulations depend on the assumed k_f and k_r. In general, when the dimer fraction is assumed small ($k_f = 10^{-6}$ s^{-1} and $k_r = 10^{-3}$ s^{-1}, so $f_{dimer} \sim 0.001$) the fractional contribution of the lower volatility components ($C^* \leq 10$ μg m^{-3}) is greater. However, when substantial dimer formation is allowed ($k_f = 10^{-3}$ s^{-1} and $k_r = 10^{-6}$ s^{-1} or $k_r = 10^{-4}$ s^{-1}), there are notable contributions from all C^* components and the dimers comprise the largest fraction. Consequently, this suggests that evaporation for these cases is controlled largely by dimer dissociation. The optimized C^* distributions from the high-dimer-fraction simulations are more consistent with the C^* distributions derived from the measured particle composition shown in Figure 2(a).

Under humid conditions, SOA evaporation behavior was best reproduced in the cases with $D_b = 10^{-16}$ m^2 s^{-1}, while the evaporation rates immediately after the dilution were slightly underestimated in the cases with $D_b = 10^{-17}$ m^2 s^{-1}. The evaporation rate was significantly underestimated in the cases with $D_b \leq 10^{-18}$ m^2 s^{-1}, suggesting that higher D_b (lower viscosity) was necessary to reproduce the observed time-dependent VFR under humid conditions. The extent and rate of dimer formation also influenced the simulation results. In particular, even in the low-viscosity case (i.e., $D_b = 10^{-16}$ m^2 s^{-1}), the evaporation rate was underestimated in the simulations with relatively fast dimer formation ($k_f = 10^{-3}$ s^{-1}) and slow dimer dissociation ($k_r = 10^{-6}$ s^{-1}) (Figure 5). However, in the simulation with relatively fast dimer formation ($k_f = 10^{-3}$ s^{-1}) and fast dimer dissociation ($k_r = 10^{-4}$ s^{-1}), the C^* distribution and SOA evaporative behavior were both consistent with observations. In the simulation with little dimer formation ($k_f = 10^{-6}$ s^{-1} and $k_r = 10^{-3}$ s^{-1}), good agreement with the evaporation profile was obtained when $D_b \geq 10^{-17}$ m^2 s^{-1}, but the optimized C^* distributions differed notably from that estimated from the particle composition.

(b) With constraint of C^* distributions

The above solutions provide general insight into the factors controlling the SOA evaporation, but are not unique owing to a lack of constraints. To better understand the factors controlling the SOA evaporative behavior, we determined optimized values of D_b, k_f, and k_r using the observation-based C^* distributions and f_{dimer} (Table 2) as a constraint. Based on chemical analysis and heat-induced evaporation experiments , Sato, et al. [33] have estimated that SOA components with relatively high volatility ($C^* \geq 10^2$ μg m^{-3}) contribute 20–50% of the total SOA from α-pinene. In addition, C^* distributions estimated in other previous studies also show that the SVOC had high contributions (33–77%), suggesting that these compounds made important contributions to the total products from α-pinene ozonolysis. These C^* distributions (f_i) were used as initial conditions, and we tolerated the variation of f_i within ± 10% from the initial values. As noted in Section 3.1, the contributions of dimers have not been adequately estimated in the literature, except by Sato, et al. [33]. Thus, the following assumptions were made in the sensitivity simulations: (1) compounds with $C^* \leq 10^{-2}$ μg m^{-3} were considered as dimers, (2) compounds with $C^* \leq 10^{-2}$ μg m^{-3} were considered as low-volatility monomers ($C^* = 10^{-1}$ μg m^{-3} is practically non-volatile in this calculation), and (3) in the case of Chhabra, et al. [32], the dimer fraction was set to be the same as or half that in Sato, et al. [33]. These assumptions are summarized in Table 2.

We minimized the RMSE between the observed and simulated SOA concentrations for the formation experiments and between the observed and simulated VFR for the dilution experiments using the Nelder-Mead simplex algorithm, as noted in Section 2.3. For the formation experiments, an optimal set k_f and $\Sigma(a_i)$ was calculated by minimizing sum of the RMSE of the observed and simulated time dependent SOA concentrations in the reaction chamber (normalized by the observed SOA concentration at the end of the formation experiments) and the RMSE of f_{dimer} at

451 the end of the formation experiments with the same weight. For the dilution experiments, an
452 optimal set k_r, D_b, and f_i was calculated by minimizing the RMSE of the observed and simulated
453 VFR in the EDC. Fitting calculations for the reaction chamber and EDC were sequentially
454 conducted. When the criteria of the RMSE for the reaction chamber and EDC were simultaneously
455 met, the fitted parameters are considered as an optimal solution. Initial values of objective variables
456 (i.e., a_i, k_f, k_r, and D_b) were pseudo-randomly chosen within plausible ranges, and these sets of
457 fitting calculations were iterated 20 times.

458 The simulated VFR during dilution-induced evaporation is summarized in Figure 6(a). In the
459 simulations with consideration of the observed fraction of dimers (CA-SA18-STD[33] and CA-
460 CH15-HighD[32] in Table 2), the observed VFR was reasonably reproduced with RMSE = 0.01. In
461 contrast, in the simulations without consideration of dimers, the observed VFR was not accurately
462 reproduced (RMSE = 0.05–0.08). As shown in Section 3.2.2 (a), the observed evaporation could
463 be reproduced by introducing large fractions of LVOC, even in the simulations unconstrained by
464 the C^* distribution. However, when constraining with these C^* distributions from the previous
465 studies, the observed VFR could not be well reproduced even after optimization of k_r and D_b. As
466 already noted, SVOC (C^* = 10^2–10^3 μg m^{-3}) made important contributions in the observation-
467 based C^* distributions (Figures 2(a)). When constraining with the C^* distributions, dimer formation
468 and decomposition appear to play important roles in SOA evaporation. This point is clearly
469 indicated in Figure 6(c). By introducing half of the observed dimer fraction (CA-CH15-HalfD),
470 the model performance (RMSE) was in between the case considering the observed dimers (59%)
471 and that not considering the dimers. The relationship between the model performance (RMSE) and
472 the estimated D_b is shown in Figure 6(d). With lower dimer fractions, the estimated D_b was lower,
473 although the observed VFR after the dilution was not adequately reproduced. In the simulations

with reasonable model performance, estimated D_b was around $10^{-17.8}$ m^2 s^{-1}. Hereafter, we mainly show the results in the case of CA-SA18-STD.

The fitting parameters in the case of CA-SA18-STD were as follows: $\log_{10}(k_f\ [s^{-1}]) = -2.8, -5.9 \leq \log_{10}(k_r\ [s^{-1}]) \leq -5.1$, and $-18.0 \leq \log_{10}(D_b\ [m^2\ s^{-1}]) \leq -17.8$ (Table 3). We should note that k_f and D_b were well constrained in relatively narrow ranges over the 20 iterations and over the three experiments under the dry conditions, while the estimated k_r indicated a variability by more than an order of magnitude. In this case, SOA evaporation was associated mostly with the evaporation of compounds with relatively high C^* ($\geq 10^2$ μg m^{-3}) and a fraction of dimer increased after the dilution (Figure 7).

In Sato, et al. [33], filter sampling was not conducted during the experiments under the humid conditions. We therefore assume that the C^* distributions are the same for the dry and humid experiments. This is reasonable given that variation in RH has little influence on the formation of low-volatility HOMs and dimers[60] or on the formation of SOA.[57, 61] Under humid conditions, the estimated fitting parameters were as follows: $-2.9 \leq \log_{10}(k_f[s^{-1}]) \leq -2.7$, $-4.0 \leq \log_{10}(k_r[s^{-1}]) \leq -3.9$, $-15.4 \leq \log_{10}(D_b[m^2\ s^{-1}]) \leq -13.3$ (Table 3). These D_b values ($\leq 10^{-16}$ m^2 s^{-1}) indicate that particle mixing is sufficiently fast (equilibrium timescale of particles with diameters of 0.1–0.4 μm was less than 1 min[19, 62]) compared to the evaporation timescale (33-46 min[33]), thus bulk diffusion was not a factor that limited evaporation under humid conditions. In contrast, bulk diffusion should inhibit evaporation under dry conditions.

Dimer dissociation rates estimated in this study were consistent with the previous estimate (10^{-5}–10^{-4} s^{-1}) based on isothermal evaporation by D'Ambro, et al. [55] Chemical analysis has shown that dimers make important contributions to SOA from monoterpene and aromatic VOC [33, 37, 55]. Dimer formation should therefore be considered for the accurate reproduction of isothermal evaporation

497 rates. Kolesar, et al. [18] have estimated a faster k_r of 1.6×10^{-3} to 2.8×10^{-2} s^{-1}, probably because
498 they used the isothermal-evaporation data of Vaden, et al. [23], which show faster evaporation than
499 those of Sato, et al. [33] and D'Ambro, et al. [55] (Figure 1(a)). There are obviously large uncertainties
500 in isothermal evaporation rates, as already discussed in Section 3.1. The cause of the differences
501 between experiments is further discussed in Section 3.2.3.

502 The D_b for dry particles estimated in this study was similar to that of Zaveri, et al. [31], who
503 estimated D_b (2×10^{-18} m^2 s^{-1}) from the experimental change of the sizes of SOA from α-pinene
504 under dry conditions (RH ~ 10%). Higher D_b values under humid conditions is also consistent with
505 previous measurements of SOA viscosity[36, 63, 64] or modeling analysis of SOA reactivity.[65, 66]
506 Shiraiwa, et al. [35] and DeRieux, et al. [36] have developed a parameterization for the estimation of
507 T_g of individual SOA compounds, as detailed in Section S5 of the SI. With the estimated T_g, the
508 dynamic viscosity (η) and D_b can be calculated from the modified Vogel–Tammann–Fulcher
509 equation and the Stokes–Einstein equation, respectively[35, 36]. These equations and estimated η and
510 D_b are summarized in Section S5 and Table S4 of the SI. The value of D_b calculated from chemical
511 composition data and an estimated T_g ($D_{b,chem}$)[35, 36] was much lower than the value of D_b estimated
512 from parameter fitting of dilution-induced evaporation rates ($D_{b,dil}$) (Table 3) under both dry and
513 humid conditions. This difference is consistent with the results of Tikkanen, et al. [67], who have
514 shown that the observed dilution-induced evaporation rate is greatly underestimated by simulations
515 using a kinetic model with $D_{b,chem}$. Tikkanen, et al. [67] have also shown that the observed dilution-
516 induced evaporation rate can be reproduced if the T_g values of all compounds are reduced to
517 account for the uncertainty of T_g within a plausible range (30 K). As shown in Table S4 of the SI,
518 the $D_{b,chem}$ derived from T_g but artificially reduced by 30 K was closer to $D_{b,dil}$ (Table 3). The
519 implication is that $D_{b,dil}$ and $D_{b,chem}$ were at least consistent within the uncertainty of T_g, though

these estimated $D_{b,chem}$ values include large uncertainty. As noted in the Introduction, DeRieux, et al. [36] derived an equation to calculate $D_{b,chem}$ from the composition of SOA (Equations S11-17 of the SI). Thus, the relationship between D_b and SOA composition can be used to simultaneously optimize $D_{b,chem}$ and C^*. However, because of the large discrepancy between $D_{b,dil}$ and $D_{b,chem}$ as shown above, we could not conduct such an optimization analysis in this study.

3.2.3. Comparison with previous studies

As already noted in Section 3.1, the dilution-induced evaporation rates used here were lower than the rates reported in most previous studies (Figure 1(a)). Differences in the treatment of VWL, the range of SOA concentrations, and SOA composition that arise from different reaction conditions are all possible explanations for the difference in SOA evaporation rates. Vaden, et al. [23] removed gaseous compounds by activated charcoal denuders. Yli-Juuti, et al. [25] used a stainless steel chamber for an evaporation chamber and assumed in their simulations that gaseous semi-volatile compounds instantaneously deposited on the walls. To estimate the impact of VWL, we compared the VFR simulated with the VWL module of Krechmer, et al. [46] and the VFR simulated with the instantaneous VWL that was assumed in previous studies[23, 25] (Figure 8). In this simulation, we used the fitted parameters a_i, k_f, k_r, and D_b estimated in Section 3.2.2 (Table 3), and we changed only the VFR calculation methods. Our simulations indicated that 3 h after the start of dilution the VFR in our experimental setups was higher than the VFR in experiments with an instantaneous VWL by about 0.06. This result indicates that treatment of the VWL range could partly explain the differences in SOA evaporation rates among the experiments. This point has also been discussed in a more general context by Li and Shiraiwa [68] based on comparison of SOA equilibrium timescales in an open system (with a constant vapor concentration) and a closed system (with a finite amount of vapor). By contrast to the above discussion, the difference of VFR after dilution

between the simulation without VWL and that with a module of Krechmer, et al. [46] was only a few percent, suggesting that contributions of VWL to the SOA evaporation in our closed system was modest. D'Ambro, et al. [55] have measured evaporation rates of SOA on filters. Quantitative assessment of the differences of the VFR between SOA suspended in the air and on filters is difficult, though such differences could also change evaporation rates after isothermal dilution. In addition, the VFR after evaporation was also sensitive to the total OA concentration. Simulations used to evaluate the sensitivity of evaporative behavior to OA concentrations just before dilution revealed that the VFR after dilution decreased by about 0.1 when the initial concentration of total product (particles + gas) was reduced by one order of magnitude with the proportional C^* distribution.

3.3. Simulations of Evaporative Behaviors of SOA from 1,3,5-TMB

During the formation experiment of 1,3,5-TMB, SOA formation did not start until after the decay of the precursor VOC. This behavior, which has already been reported[69], could be accounted for by several explanations, including dependence of SOA yields on NO_x concentrations because of differences of chemical pathways[70] or differences of induction periods before SOA formation.[71] Ng, et al. [70] have shown that the presence of NO initially suppresses the formation of SOA from aromatic VOC. In this study, we simply set $a_i = 0$ when the NO concentration was higher than the critical concentration (fitting parameter). This parameter setting might not represent the actual mechanism of SOA formation, though this choice of a_i had little influence on the simulation of SOA evaporation by isothermal dilution.

As already noted in Section 3.1, evaporation rates and C^* distributions were similar for dry SOA from α-pinene and 1,3,5-TMB. The estimated parameters of k_f, k_r, and D_b were likewise similar to

each other as well (Table 3). The estimated values among several experiments were as follows: $-18.6 \leq \log_{10}(D_b\ [m^2\ s^{-1}]) \leq -18.1$ and $-8.3 \leq \log_{10}(k_r\ [s^{-1}]) \leq -3.7$.

Comparisons of evaporation rates or viscosities between SOA from monoterpene (mostly α-pinene) and aromatic VOC (toluene, xylene, or TMB) have recently been conducted. These rates continue to be a controversial issue. Based on the bead-mobility technique,[72] it has been shown that the viscosity of SOA particles is higher under dry condition than under humid condition for the SOA from α-pinene[73] and toluene.[63] The D_b values for the SOA from α-pinene and toluene were estimated previously to be very low (10^{-20} m^2 s^{-1}) under dry conditions. However, other groups have shown that diffusion of the SOA from monoterpene and aromatic VOC behaves differently when based on measurements of evaporation rates from organic films[74] or measurements of the mixing state of isotopically labeled SOA.[54] In both cases,[54, 74] evaporation of the SOA from α-pinene was not diffusion limited under either dry nor humid conditions, whereas the SOA from aromatic VOC (toluene or m-xylene) are diffusion limited under dry conditions but not under humid conditions. The above-mentioned studies were consistent with respect to the behavior of diffusion of the SOA from aromatic VOC, though they were inconsistent with respect to the behavior of diffusion of the SOA from α-pinene under dry conditions. Our results indicated that evaporation of the SOA from α-pinene was diffusion limited under dry conditions. This behavior is consistent with the viscosity estimates based on the poke-flow technique[73] or particle formation experiments,[31] but inconsistent when based on measurements of evaporation rates of organic films[74] and SOA mixing experiments.[54] DeRieux, et al. [36] have shown that the viscosity of dry SOA from toluene (10^9–10^{12} Pa s) are higher than that of dry SOA from α-pinene (10^7–10^{10} Pa s). Thresholds of diffusion limitation might differ among methodologies, and SOA properties

could differ because of factors other than precursor types (e.g., concentrations or presence of oxidants). These differences might account for the different conclusions.

The SOA yields and O:C ratios of mixtures of anthropogenic and biogenic SOA are seemingly explained as a linear combination of properties of purely anthropogenic and biogenic SOA.[48, 75] However, other studies[41, 76] have shown that SOA yields cannot be represented by linear combinations of different types of SOA, probably due to the nonlinear chemistry of the HOMs, dimer formation, and/or cycles of radicals. The evaporative behavior of these SOA mixtures should therefore be the focus of future studies.

4. Conclusions

We have previously measured the evaporative behavior of SOA from α-pinene ozonolysis and 1,3,5-TMB/NO_x photooxidation by conducting isothermal dilution experiments.[33, 37] We have also measured the volatility distributions of the SOA based on chemical analyses using LC-TOF-MS. These observations, which have revealed that the distributions of SOA volatility estimated from SOA yield curves during formation experiments, isothermal dilution experiments, and chemical analysis all differ, suggest that it is important to model the multi-generational gas- and particle-phase reactions to produce ELVOC and LVOC along with the kinetics in gas-particle conversion if we are to explain these differences. In this study, we conducted model simulations using the VBS framework with consideration of kinetic gas-particle partitioning, formation and dissociation of dimers, and limitation by particle-phase diffusion to understand the evaporative behaviors of SOA from biogenic and aromatic VOC and their controlling factors.

SOA evaporation rates after dilution were particularly sensitive to C^* distributions, though k_f, k_r, and D_b were also important factors that controlled the evaporation rates. Generally, C^* and k_f

611 determined equilibrium concentrations after evaporation, whereas k_r and D_b determined mainly
612 equilibration timescales. Fitting of the observed SOA formation and evaporation rates could not
613 produce unique solutions of all these parameters because the observed time-dependent VFR could
614 be reproduced by optimizing C^* distributions with different sets of k_f, k_r, and D_b. We then used the
615 various C^* distributions estimated from chemical analysis or heating experiments as a constraint,
616 and in this way we estimated k_f, k_r, and D_b. Among the various C^* distributions, the observed
617 evaporation behavior could be reproduced in the experiment with significant dimer contributions
618 (59%) and low D_b ($10^{-17.8}$ m^2 s^{-1}). These results suggest that both dimerization and bulk diffusion
619 contributed to the observed slow evaporation rates under dry conditions. By contrast, particle-
620 phase diffusion did not practically inhibit SOA evaporation under humid conditions. This
621 dependence on RH was consistent with some previous studies. However, several previous studies
622 have shown that evaporation of α-pinene SOA is not diffusion limited under dry conditions, but
623 that evaporation of aromatic SOA is diffusion limited. The reason for this difference of diffusion
624 limitation has not yet been resolved, and it should be examined in future studies. We also found
625 that model parameters estimated for the SOA from 1,3,5-TMB were similar to those estimated for
626 the SOA from α-pinene under dry conditions. The implication is that dimer formation and bulk
627 diffusivity are important in reproducing evaporative behaviors of both biogenic and aromatic SOA.
628 Evaporation rates of SOA from α-pinene varied among experiments. These variations could be
629 partly explained by differences in the treatment of the VWL. The experimental design is thus a
630 critical consideration in the simulation of SOA evaporative behavior.
631

632 ASSOCIATED CONTENT

633 **Supporting Information**

The Supporting Information is available free of charge on the ACS Publications website.

AUTHOR INFORMATION

Corresponding Author

* E-mail: morino.yu@nies.go.jp

Notes

The authors declare no competing financial interest.

ACKNOWLEDGMENTS

This research was supported by the Environment Research and Technology Development Fund (JPMEERF20185001, JPMEERF20145008, JPMEERF14S11201) of the Ministry of the Environment, Japan and the Grants-in-Aid for Scientific Research (JP16H06305) of the Japan Society for the Promotion of Science. The authors acknowledge Gabriel Isaacman-VanWertz (VT) for providing the experimental data.

REFERENCES

1. Zhang, Q.; Jimenez, J. L.; Canagaratna, M. R.; Allan, J. D.; Coe, H.; Ulbrich, I.; Alfarra, M. R.; Takami, A.; Middlebrook, A. M.; Sun, Y. L.; Dzepina, K.; Dunlea, E.; Docherty, K.; DeCarlo, P. F.; Salcedo, D.; Onasch, T.; Jayne, J. T.; Miyoshi, T.; Shimono, A.; Hatakeyama, S.; Takegawa, N.; Kondo, Y.; Schneider, J.; Drewnick, F.; Borrmann, S.; Weimer, S.; Demerjian, K.; Williams, P.; Bower, K.; Bahreini, R.; Cottrell, L.; Griffin, R. J.; Rautiainen, J.; Sun, J. Y.; Zhang, Y. M.; Worsnop, D. R., Ubiquity and dominance of oxygenated species in organic aerosols in anthropogenically-influenced Northern Hemisphere midlatitudes. *Geophys. Res. Lett.* **2007,** *34*

(13), L13801.
2. Hallquist, M.; Wenger, J. C.; Baltensperger, U.; Rudich, Y.; Simpson, D.; Claeys, M.; Dommen, J.; Donahue, N. M.; George, C.; Goldstein, A. H.; Hamilton, J. F.; Herrmann, H.; Hoffmann, T.; Iinuma, Y.; Jang, M.; Jenkin, M. E.; Jimenez, J. L.; Kiendler-Scharr, A.; Maenhaut, W.; McFiggans, G.; Mentel, T. F.; Monod, A.; Prevot, A. S. H.; Seinfeld, J. H.; Surratt, J. D.; Szmigielski, R.; Wildt, J., The formation, properties and impact of secondary organic aerosol: current and emerging issues. *Atmos. Chem. Phys.* **2009,** *9* (14), 5155-5236.
3. Noziere, B.; Kaberer, M.; Claeys, M.; Allan, J.; D'Anna, B.; Decesari, S.; Finessi, E.; Glasius, M.; Grgic, I.; Hamilton, J. F.; Hoffmann, T.; Iinuma, Y.; Jaoui, M.; Kahno, A.; Kampf, C. J.; Kourtchev, I.; Maenhaut, W.; Marsden, N.; Saarikoski, S.; Schnelle-Kreis, J.; Surratt, J. D.; Szidat, S.; Szmigielski, R.; Wisthaler, A., The Molecular Identification of Organic Compounds in the Atmosphere: State of the Art and Challenges. *Chemical Reviews* **2015,** *115* (10), 3919-3983.
4. Saunders, S. M.; Jenkin, M. E.; Derwent, R. G.; Pilling, M. J., Protocol for the development of the Master Chemical Mechanism, MCM v3 (Part A): tropospheric degradation of non-aromatic volatile organic compounds. *Atmos. Chem. Phys.* **2003,** *3*, 161-180.
5. Li, J. Y.; Cleveland, M.; Ziemba, L. D.; Griffin, R. J.; Barsanti, K. C.; Pankow, J. F.; Ying, Q., Modeling regional secondary organic aerosol using the Master Chemical Mechanism. *Atmos. Environ.* **2015,** *102*, 52-61.
6. Aumont, B.; Szopa, S.; Madronich, S., Modelling the evolution of organic carbon during its gas-phase tropospheric oxidation: development of an explicit model based on a self generating approach. *Atmos. Chem. Phys.* **2005,** *5*, 2497-2517.
7. Camredon, M.; Aumont, B.; Lee-Taylor, J.; Madronich, S., The SOA/VOC/NOx system: an explicit model of secondary organic aerosol formation. *Atmos. Chem. Phys.* **2007,** *7* (21), 5599-5610.
8. Donahue, N. M.; Epstein, S. A.; Pandis, S. N.; Robinson, A. L., A two-dimensional volatility basis set: 1. organic-aerosol mixing thermodynamics. *Atmos. Chem. Phys.* **2011,** *11* (7), 3303-3318.
9. Donahue, N. M.; Robinson, A. L.; Stanier, C. O.; Pandis, S. N., Coupled partitioning, dilution, and chemical aging of semivolatile organics. *Environ Sci Technol* **2006,** *40* (8), 02635-2643.
10. Cappa, C. D.; Zhang, X.; Loza, C. L.; Craven, J. S.; Yee, L. D.; Seinfeld, J. H., Application of the Statistical Oxidation Model (SOM) to Secondary Organic Aerosol formation from photooxidation of C-12 alkanes. *Atmos. Chem. Phys.* **2013,** *13* (3), 1591-1606.
11. Zhang, X.; Seinfeld, J. H., A functional group oxidation model (FGOM) for SOA formation and aging. *Atmos. Chem. Phys.* **2013,** *13* (12), 5907-5926.
12. Ehn, M.; Thornton, J. A.; Kleist, E.; Sipila, M.; Junninen, H.; Pullinen, I.; Springer, M.; Rubach, F.; Tillmann, R.; Lee, B.; Lopez-Hilfiker, F.; Andres, S.; Acir, I. H.; Rissanen, M.; Jokinen, T.; Schobesberger, S.; Kangasluoma, J.; Kontkanen, J.; Nieminen, T.; Kurten, T.; Nielsen, L. B.; Jorgensen, S.; Kjaergaard, H. G.; Canagaratna, M.; Dal Maso, M.; Berndt, T.; Petaja, T.; Wahner, A.; Kerminen, V. M.; Kulmala, M.; Worsnop, D. R.; Wildt, J.; Mentel, T. F., A large source of low-volatility secondary organic aerosol. *Nature* **2014,** *506* (7489), 476-479.
13. Zhang, X.; Mcvay, R. C.; Huang, D. D.; Dalleska, N. F.; Aumont, B.; Flagan, R. C.; Seinfeld, J. H., Formation and evolution of molecular products in alpha-pinene secondary organic aerosol. *P Natl Acad Sci USA* **2015,** *112* (46), 14168-14173.
14. Zhang, X.; Lambe, A. T.; Upshur, M. A.; Brooks, W. A.; Be, A. G.; Thomson, R. J.;

Geiger, F. M.; Surratt, J. D.; Zhang, Z. F.; Gold, A.; Graf, S.; Cubison, M. J.; Groessl, M.; Jayne, J. T.; Worsnop, D. R.; Canagaratna, M. R., Highly Oxygenated Multifunctional Compounds in alpha-Pinene Secondary Organic Aerosol. *Environ Sci Technol* **2017,** *51* (11), 5932-5940.
15. Kalberer, M.; Paulsen, D.; Sax, M.; Steinbacher, M.; Dommen, J.; Prevot, A. S. H.; Fisseha, R.; Weingartner, E.; Frankevich, V.; Zenobi, R.; Baltensperger, U., Identification of polymers as major components of atmospheric organic aerosols. *Science* **2004,** *303* (5664), 1659-1662.
16. Kourtchev, I.; Doussin, J. F.; Giorio, C.; Mahon, B.; Wilson, E. M.; Maurin, N.; Pangui, E.; Venables, D. S.; Wenger, J. C.; Kalberer, M., Molecular composition of fresh and aged secondary organic aerosol from a mixture of biogenic volatile compounds: a high-resolution mass spectrometry study. *Atmospheric Chemistry and Physics* **2015,** *15* (10), 5683-5695.
17. Trump, E. R.; Donahue, N. M., Oligomer formation within secondary organic aerosols: equilibrium and dynamic considerations. *Atmos. Chem. Phys.* **2014,** *14* (7), 3691-3701.
18. Kolesar, K. R.; Chen, C.; Johnson, D.; Cappa, C. D., The influences of mass loading and rapid dilution of secondary organic aerosol on particle volatility. *Atmospheric Chemistry and Physics* **2015,** *15* (16), 9327-9343.
19. Zaveri, R. A.; Easter, R. C.; Shilling, J. E.; Seinfeld, J. H., Modeling kinetic partitioning of secondary organic aerosol and size distribution dynamics: representing effects of volatility, phase state, and particle-phase reaction. *Atmos. Chem. Phys.* **2014,** *14* (10), 5153-5181.
20. Roldin, P.; Eriksson, A. C.; Nordin, E. Z.; Hermansson, E.; Mogensen, D.; Rusanen, A.; Boy, M.; Swietlicki, E.; Svenningsson, B.; Zelenyuk, A.; Pagels, J., Modelling non-equilibrium secondary organic aerosol formation and evaporation with the aerosol dynamics, gas- and particle-phase chemistry kinetic multilayer model ADCHAM. *Atmos. Chem. Phys.* **2014,** *14* (15), 7953-7993.
21. Carlton, A. G.; Bhave, P. V.; Napelenok, S. L.; Edney, E. D.; Sarwar, G.; Pinder, R. W.; Pouliot, G. A.; Houyoux, M., Model Representation of Secondary Organic Aerosol in CMAQv4.7. *Environ Sci Technol* **2010,** *44* (22), 8553-8560.
22. Tsigaridis, K.; Daskalakis, N.; Kanakidou, M.; Adams, P. J.; Artaxo, P.; Bahadur, R.; Balkanski, Y.; Bauer, S. E.; Bellouin, N.; Benedetti, A.; Bergman, T.; Berntsen, T. K.; Beukes, J. P.; Bian, H.; Carslaw, K. S.; Chin, M.; Curci, G.; Diehl, T.; Easter, R. C.; Ghan, S. J.; Gong, S. L.; Hodzic, A.; Hoyle, C. R.; Iversen, T.; Jathar, S.; Jimenez, J. L.; Kaiser, J. W.; Kirkevag, A.; Koch, D.; Kokkola, H.; Lee, Y. H.; Lin, G.; Liu, X.; Luo, G.; Ma, X.; Mann, G. W.; Mihalopoulos, N.; Morcrette, J. J.; Muller, J. F.; Myhre, G.; Myriokefalitakis, S.; Ng, N. L.; O'Donnell, D.; Penner, J. E.; Pozzoli, L.; Pringle, K. J.; Russell, L. M.; Schulz, M.; Sciare, J.; Seland, O.; Shindell, D. T.; Sillman, S.; Skeie, R. B.; Spracklen, D.; Stavrakou, T.; Steenrod, S. D.; Takemura, T.; Tiitta, P.; Tilmes, S.; Tost, H.; van Noije, T.; van Zyl, P. G.; von Salzen, K.; Yu, F.; Wang, Z.; Wang, Z.; Zaveri, R. A.; Zhang, H.; Zhang, K.; Zhang, Q.; Zhang, X., The AeroCom evaluation and intercomparison of organic aerosol in global models. *Atmos. Chem. Phys.* **2014,** *14* (19), 10845-10895.
23. Vaden, T. D.; Imre, D.; Beranek, J.; Shrivastava, M.; Zelenyuk, A., Evaporation kinetics and phase of laboratory and ambient secondary organic aerosol. *Proc. Natl. Acad. Sci. U. S. A.* **2011,** *108* (6), 2190-2195.
24. Wilson, J.; Imre, D.; Beranek, J.; Shrivastava, M.; Zelenyuk, A., Evaporation Kinetics of Laboratory-Generated Secondary Organic Aerosols at Elevated Relative Humidity. *Environ Sci Technol* **2015,** *49* (1), 243-249.
25. Yli-Juuti, T.; Pajunoja, A.; Tikkanen, O. P.; Buchholz, A.; Faiola, C.; Vaisanen, O.; Hao,

749 L. Q.; Kari, E.; Perakyla, O.; Garmash, O.; Shiraiwa, M.; Ehn, M.; Lehtinen, K.; Virtanen, A.,
750 Factors controlling the evaporation of secondary organic aerosol from alpha-pinene ozonolysis.
751 *Geophys. Res. Lett.* **2017,** *44* (5), 2562-2570.
752 26. Saleh, R.; Donahue, N. M.; Robinson, A. L., Time Scales for Gas-Particle Partitioning
753 Equilibration of Secondary Organic Aerosol Formed from Alpha-Pinene Ozonolysis. *Environ Sci*
754 *Technol* **2013,** *47* (11), 5588-5594.
755 27. Saha, P. K.; Grieshop, A. P., Exploring Divergent Volatility Properties from Yield and
756 Thermodenuder Measurements of Secondary Organic Aerosol from alpha-Pinene Ozonolysis.
757 *Environ Sci Technol* **2016,** *50* (11), 5740-5749.
758 28. Li, Y.; Poschl, U.; Shiraiwa, M., Molecular corridors and parameterizations of volatility in
759 the chemical evolution of organic aerosols. *Atmos. Chem. Phys.* **2016,** *16* (5), 3327-3344.
760 29. Shiraiwa, M.; Berkemeier, T.; Schilling-Fahnestock, K. A.; Seinfeld, J. H.; Poschl, U.,
761 Molecular corridors and kinetic regimes in the multiphase chemical evolution of secondary organic
762 aerosol. *Atmos. Chem. Phys.* **2014,** *14* (16), 8323-8341.
763 30. Stark, H.; Yatavelli, R. L. N.; Thompson, S. L.; Kang, H.; Krechmer, J. E.; Kimmel, J.
764 R.; Palm, B. B.; Hu, W. W.; Hayes, P. L.; Day, D. A.; Campuzano-Jost, P.; Canagaratna, M. R.;
765 Jayne, J. T.; Worsnop, D. R.; Jimenez, J. L., Impact of Thermal Decomposition on Thermal
766 Desorption Instruments: Advantage of Thermogram Analysis for Quantifying Volatility
767 Distributions of Organic Species. *Environmental Science & Technology* **2017,** *51* (15), 8491-8500.
768 31. Zaveri, R. A.; Shilling, J. E.; Zelenyuk, A.; Liu, J.; Bell, D. M.; D'Ambro, E. L.; Gaston,
769 C. J.; Thornton, J. A.; Laskin, A.; Lin, P.; Wilson, J.; Easter, R. C.; Wang, J.; Bertram, A. K.;
770 Martin, S. T.; Seinfeld, J. H.; Worsnop, D. R., Growth Kinetics and Size Distribution Dynamics
771 of Viscous Secondary Organic Aerosol. *Environ Sci Technol* **2018,** *52* (3), 1191-1199.
772 32. Chhabra, P. S.; Lambe, A. T.; Canagaratna, M. R.; Stark, H.; Jayne, J. T.; Onasch, T. B.;
773 Davidovits, P.; Kimmel, J. R.; Worsnop, D. R., Application of high-resolution time-of-flight
774 chemical ionization mass spectrometry measurements to estimate volatility distributions of alpha-
775 pinene and naphthalene oxidation products. *Atmospheric Measurement Techniques* **2015,** *8* (1), 1-
776 18.
777 33. Sato, K.; Fujitani, Y.; Inomata, S.; Morino, Y.; Tanabe, K.; Ramasamy, S.; Hikida, T.;
778 Shimono, A.; Takami, A.; Fushimi, A.; Kondo, Y.; Imamura, T.; Tanimoto, H.; Sugata, S.,
779 Studying volatility from composition, dilution, and heating measurements of secondary organic
780 aerosols formed during alpha-pinene ozonolysis. *Atmos. Chem. Phys.* **2018,** *18* (8), 5455-5466.
781 34. Isaacman-VanWertz, G.; Massoli, P.; O'Brien, R.; Lim, C.; Franklin, J. P.; Moss, J. A.;
782 Hunter, J. F.; Nowak, J. B.; Canagaratna, M. R.; Misztal, P. K.; Arata, C.; Roscioli, J. R.;
783 Herndon, S. T.; Onasch, T. B.; Lambe, A. T.; Jayne, J. T.; Su, L.; Knopf, D. A.; Goldstein, A.
784 H.; Worsnop, D. R.; Kroll, J. H., Chemical evolution of atmospheric organic carbon over multiple
785 generations of oxidation. *Nat Chem* **2018,** *10* (4), 462-468.
786 35. Shiraiwa, M.; Li, Y.; Tsimpidi, A. P.; Karydis, V. A.; Berkemeier, T.; Pandis, S. N.;
787 Lelieveld, J.; Koop, T.; Poschl, U., Global distribution of particle phase state in atmospheric
788 secondary organic aerosols. *Nature Communications* **2017,** *8*, 1-7.
789 36. DeRieux, W.-S. W.; Li, Y.; Lin, P.; Laskin, J.; Laskin, A.; Bertram, A. K.; Nizkorodov,
790 S. A.; Shiraiwa, M., Predicting the glass transition temperature and viscosity of secondary organic
791 material using molecular composition. *Atmospheric Chemistry and Physics* **2018,** *18* (9), 6331-
792 6351.
793 37. Sato, K.; Fujitani, Y.; Inomata, S.; Morino, Y.; Tanabe, K.; Hikida, T.; Shimono, A.;
794 Takami, A.; Fushimi, A.; Kondo, Y.; Imamura, T.; Tanimoto, H.; Sugata, S., A study of volatility

by composition, heating, and dilution measurements of secondary organic aerosol from 1,3,5-trimethylbenzene. *Atmos. Chem. Phys.* **2019,** *19* (23), 14901-14915.
38. Morino, Y.; Ueda, K.; Takami, A.; Nagashima, T.; Tanabe, K.; Sato, K.; Noguchi, T.; Ariga, T.; Matsuhashi, K.; Ohara, T., Sensitivities of Simulated Source Contributions and Health Impacts of PM2.5 to Aerosol Models. *Environ Sci Technol* **2017,** *51* (24), 14273-14282.
39. Al-Naiema, I. M.; Hettiyadura, A. P. S.; Wallace, H. W.; Sanchez, N. P.; Madler, C. J.; Cevik, B. K.; Bui, A. A. T.; Kettler, J.; Griffin, R. J.; Stone, E. A., Source apportionment of fine particulate matter in Houston, Texas: insights to secondary organic aerosols. *Atmos. Chem. Phys.* **2018,** *18* (21), 15601-15622.
40. Hilal, S. H.; Karickhoff, S. W.; Carreira, L. A., Prediction of the vapor pressure boiling point, heat of vaporization and diffusion coefficient of organic compounds. *Qsar Comb Sci* **2003,** *22* (6), 565-574.
41. McFiggans, G.; Mentel, T. F.; Wildt, J.; Pullinen, I.; Kang, S.; Kleist, E.; Schmitt, S.; Springer, M.; Tillmann, R.; Wu, C.; Zhao, D.; Hallquist, M.; Faxon, C.; Le Breton, M.; Hallquist, A. M.; Simpson, D.; Bergstrom, R.; Jenkin, M. E.; Ehn, M.; Thornton, J. A.; Alfarra, M. R.; Bannan, T. J.; Percival, C. J.; Priestley, M.; Topping, D.; Kiendler-Scharr, A., Secondary organic aerosol reduced by mixture of atmospheric vapours. *Nature* **2019,** *565* (7741), 587-593.
42. Liu, X. X.; Day, D. A.; Krechmer, J. E.; Brown, W.; Peng, Z.; Ziemann, P. J.; Jimenez, J. L., Direct measurements of semi-volatile organic compound dynamics show near-unity mass accommodation coefficients for diverse aerosols. *Commun Chem* **2019,** *2*, 1-9.
43. DePalma, J. W.; Horan, A. J.; Hall, W. A.; Johnston, M. V., Thermodynamics of oligomer formation: implications for secondary organic aerosol formation and reactivity. *Physical Chemistry Chemical Physics* **2013,** *15* (18), 6935-6944.
44. Claflin, M. S.; Ziemann, P. J., Thermal desorption behavior of hemiacetal, acetal, ether, and ester oligomers. *Aerosol Science and Technology* **2019,** *53* (4), 473-484.
45. Giechaskiel, B.; Ntziachristos, L.; Samaras, Z., Effect of ejector dilutors on measurements of automotive exhaust gas aerosol size distributions. *Meas Sci Technol* **2009,** *20* (4), 045703.
46. Krechmer, J. E.; Pagonis, D.; Ziemann, P. J.; Jimenez, J. L., Quantification of Gas-Wall Partitioning in Teflon Environmental Chambers Using Rapid Bursts of Low-Volatility Oxidized Species Generated in Situ. *Environ Sci Technol* **2016,** *50* (11), 5757-5765.
47. Lagarias, J. C.; Reeds, J. A.; Wright, M. H.; Wright, P. E., Convergence properties of the Nelder-Mead simplex method in low dimensions. *Siam J Optimiz* **1998,** *9* (1), 112-147.
48. Emanuelsson, E. U.; Hallquist, M.; Kristensen, K.; Glasius, M.; Bohn, B.; Fuchs, H.; Kammer, B.; Kiendler-Scharr, A.; Nehr, S.; Rubach, F.; Tillmann, R.; Wahner, A.; Wu, H. C.; Mentel, T. F., Formation of anthropogenic secondary organic aerosol (SOA) and its influence on biogenic SOA properties. *Atmospheric Chemistry and Physics* **2013,** *13* (5), 2837-2855.
49. Loza, C. L.; Coggon, M. M.; Nguyen, T. B.; Zuend, A.; Flagan, R. C.; Seinfeld, J. H., On the Mixing and Evaporation of Secondary Organic Aerosol Components. *Environ Sci Technol* **2013,** *47* (12), 6173-6180.
50. Kolesar, K. R.; Li, Z. Y.; Wilson, K. R.; Cappa, C. D., Heating-Induced Evaporation of Nine Different Secondary Organic Aerosol Types. *Environ Sci Technol* **2015,** *49* (20), 12242-12252.
51. Zhao, D. F.; Kaminski, M.; Schlag, P.; Fuchs, H.; Acir, I. H.; Bohn, B.; Häseler, R.; Kiendler-Scharr, A.; Rohrer, F.; Tillmann, R.; Wang, M. J.; Wegener, R.; Wildt, J.; Wahner, A.; Mentel, T. F., Secondary organic aerosol formation from hydroxyl radical oxidation and ozonolysis of monoterpenes. *Atmospheric Chemistry and Physics* **2015,** *15* (2), 991-1012.

52. Lambe, A. T.; Chhabra, P. S.; Onasch, T. B.; Brune, W. H.; Hunter, J. F.; Kroll, J. H.; Cummings, M. J.; Brogan, J. F.; Parmar, Y.; Worsnop, D. R.; Kolb, C. E.; Davidovits, P., Effect of oxidant concentration, exposure time, and seed particles on secondary organic aerosol chemical composition and yield. *Atmospheric Chemistry and Physics* **2015,** *15* (6), 3063-3075.
53. Bruns, E. A.; El Haddad, I.; Keller, A.; Klein, F.; Kumar, N. K.; Pieber, S. M.; Corbin, J. C.; Slowik, J. G.; Brune, W. H.; Baltensperger, U.; Prevot, A. S. H., Inter-comparison of laboratory smog chamber and flow reactor systems on organic aerosol yield and composition. *Atmospheric Measurement Techniques* **2015,** *8* (6), 2315-2332.
54. Ye, Q.; Robinson, E. S.; Ding, X.; Ye, P.; Sullivan, R. C.; Donahue, N. M., Mixing of secondary organic aerosols versus relative humidity. *Proc Natl Acad Sci U S A* **2016,** *113* (45), 12649-12654.
55. D'Ambro, E. L.; Schobesberger, S.; Zaveri, R. A.; Shilling, J. E.; Lee, B. H.; Lopez-Hilfiker, F. D.; Mohr, C.; Thornton, J. A., Isothermal Evaporation of alpha-Pinene Ozonolysis SOA: Volatility, Phase State, and Oligomeric Composition. *Acs Earth Space Chem* **2018,** *2* (10), 1058-1067.
56. Grieshop, A. P.; Donahue, N. M.; Robinson, A. L., Is the gas-particle partitioning in alpha-pinene secondary organic aerosol reversible? *Geophys. Res. Lett.* **2007,** *34* (14), L14810.
57. Kristensen, K.; Watne, Å. K.; Hammes, J.; Lutz, A.; Petäjä, T.; Hallquist, M.; Bilde, M.; Glasius, M., High-Molecular Weight Dimer Esters Are Major Products in Aerosols from α-Pinene Ozonolysis and the Boreal Forest. *Environmental Science & Technology Letters* **2016,** *3* (8), 280-285.
58. Hall, W. A.; Johnston, M. V., The Thermal-Stability of Oligomers in Alpha-Pinene Secondary Organic Aerosol. *Aerosol Sci. Technol.* **2012,** *46* (9), 983-989.
59. Cappa, C. D.; Wilson, K. R., Evolution of organic aerosol mass spectra upon heating: implications for OA phase and partitioning behavior. *Atmos. Chem. Phys.* **2011,** *11* (5), 1895-1911.
60. Li, X.; Chee, S.; Hao, J.; Abbatt, J. P. D.; Jiang, J.; Smith, J. N., Relative humidity effect on the formation of highly oxidized molecules and new particles during monoterpene oxidation. *Atmospheric Chemistry and Physics* **2019,** *19* (3), 1555-1570.
61. Wang, N.; Kostenidou, E.; Donahue, N. M.; Pandis, S. N., Multi-generation chemical aging of α-pinene ozonolysis products by reactions with OH. *Atmospheric Chemistry and Physics* **2018,** *18* (5), 3589-3601.
62. Koop, T.; Bookhold, J.; Shiraiwa, M.; Poschl, U., Glass transition and phase state of organic compounds: dependency on molecular properties and implications for secondary organic aerosols in the atmosphere. *Physical Chemistry Chemical Physics* **2011,** *13* (43), 19238-19255.
63. Song, M.; Liu, P. F.; Hanna, S. J.; Zaveri, R. A.; Potter, K.; You, Y.; Martin, S. T.; Bertram, A. K., Relative humidity-dependent viscosity of secondary organic material from toluene photo-oxidation and possible implications for organic particulate matter over megacities. *Atmospheric Chemistry and Physics* **2016,** *16* (14), 8817-8830.
64. Ullmann, D. A.; Hinks, M. L.; Maclean, A. M.; Butenhoff, C. L.; Grayson, J. W.; Barsanti, K.; Jimenez, J. L.; Nizkorodov, S. A.; Kamal, S.; Bertram, A. K., Viscosities, diffusion coefficients, and mixing times of intrinsic fluorescent organic molecules in brown limonene secondary organic aerosol and tests of the Stokes–Einstein equation. *Atmospheric Chemistry and Physics* **2019,** *19* (3), 1491-1503.
65. Li, Z. Y.; Smith, K. A.; Cappa, C. D., Influence of relative humidity on the heterogeneous oxidation of secondary organic aerosol. *Atmospheric Chemistry and Physics* **2018,** *18* (19), 14585-14608.

66. Shiraiwa, M.; Ammann, M.; Koop, T.; Poschl, U., Gas uptake and chemical aging of semisolid organic aerosol particles. *P Natl Acad Sci USA* **2011,** *108* (27), 11003-11008.
67. Tikkanen, O.-P.; Buchholz, A.; Ylisirniö, A.; Schobesberger, S.; Virtanen, A.; Yli-Juuti, T., Comparing SOA volatility distributions derived from isothermal SOA particle evaporation data and FIGAERO-CIMS measurements. *Atmospheric Chemistry and Physics Discussions* **2019**, 1-34.
68. Li, Y.; Shiraiwa, M., Timescales of secondary organic aerosols to reach equilibrium at various temperatures and relative humidities. *Atmospheric Chemistry and Physics* **2019,** *19* (9), 5959-5971.
69. Sato, K.; Hatakeyama, S.; Imamura, T., Secondary organic aerosol formation during the photooxidation of toluene: NOx dependence of chemical composition. *Journal of Physical Chemistry A* **2007,** *111* (39), 9796-9808.
70. Ng, N. L.; Kroll, J. H.; Chan, A. W. H.; Chhabra, P. S.; Flagan, R. C.; Seinfeld, J. H., Secondary organic aerosol formation from m-xylene, toluene, and benzene. *Atmos. Chem. Phys.* **2007,** *7* (14), 3909-3922.
71. Shakya, K. M.; Griffin, R. J., Secondary Organic Aerosol from Photooxidation of Polycyclic Aromatic Hydrocarbons. *Environ Sci Technol* **2010,** *44* (21), 8134-8139.
72. Renbaum-Wolff, L.; Grayson, J. W.; Bertram, A. K., Technical Note: New methodology for measuring viscosities in small volumes characteristic of environmental chamber particle samples. *Atmospheric Chemistry and Physics* **2013,** *13* (2), 791-802.
73. Renbaum-Wolff, L.; Grayson, J. W.; Bateman, A. P.; Kuwata, M.; Sellier, M.; Murray, B. J.; Shilling, J. E.; Martin, S. T.; Bertram, A. K., Viscosity of alpha-pinene secondary organic material and implications for particle growth and reactivity. *Proc Natl Acad Sci U S A* **2013,** *110* (20), 8014-9.
74. Liu, P.; Li, Y. J.; Wang, Y.; Gilles, M. K.; Zaveri, R. A.; Bertram, A. K.; Martin, S. T., Lability of secondary organic particulate matter. *Proc Natl Acad Sci U S A* **2016,** *113* (45), 12643-12648.
75. Hildebrandt, L.; Henry, K. M.; Kroll, J. H.; Worsnop, D. R.; Pandis, S. N.; Donahue, N. M., Evaluating the Mixing of Organic Aerosol Components Using High-Resolution Aerosol Mass Spectrometry. *Environ Sci Technol* **2011,** *45* (15), 6329-6335.
76. Kari, E.; Hao, L. Q.; Ylisirnio, A.; Buchholz, A.; Leskinen, A.; Yli-Pirila, P.; Nuutinen, I.; Kuuspalo, K.; Jokiniemi, J.; Faiola, C. L.; Schobesberger, S.; Virtanen, A., Potential dual effect of anthropogenic emissions on the formation of biogenic secondary organic aerosol (BSOA). *Atmospheric Chemistry and Physics* **2019,** *19* (24), 15651-15671.

Table 1. Experimental setups. $[X]_0$ indicates initial concentrations of species X.

Exp, #	Precursor	RH	$[HC]_0$ ppb	$[O_3]_0$ ppb	$[Et_2O]$ ppm	$[NO]_0$ ppb	$[NO_2]_0$ ppb	$[CH_3ONO]_0$ ppb	Dilution Ratio
1	α-pinene	<1%	839	949	32				75
2	α-pinene	<1%	544	1023	23				20
3	α-pinene	<1%	510	1078	23				43
4	α-pinene	40%	455	1091	23				33
5	α-pinene	40%	455	1091	23				20
6	α-pinene	40%	455	1091	23				77
7	1,3,5-TMB	<1%	1500			1208	30	10	20
8	1,3,5-TMB	<1%	1526			1214	7	10	40
9	1,3,5-TMB	<1%	1515			1195	14	10	63
10	1,3,5-TMB	<1%	1488			1203	6	10	86

Abbreviations: RH: relative humidity, HC: hydrocarbon, Et_2O: diethyl ether, TMB: trimethylbenzene.

Table 2. List of C^* distributions estimated from chemical analysis and heating experiments in previous studies. Experiments examining secondary organic aerosol from ozonolysis of α-pinene were selected, and details of these estimates are provided in Section S3 of the SI.

Distribution name	Method	System	Relative humidity	Dimer fraction	Reference
CA_SA18_STD	Chemical analysis (offline ESI-LC-TOF-MS & parameterization of C^*)	Smog chamber	≤1% and 40%	59%	Sato, et al. [33]
CA_SA18_halfD	"[a]	"	"	30%	"
HE_SA18_wD	Heating experiments (TD-AMS)	"	"	18%	Sato, et al. [33]
HE_SA18_woD	"	"	"	0%	"
CA_CH15_ wD	Chemical analysis (online-CIMS & parameterization of C^*)	PAM flow reactor	30%	11%	Chhabra, et al. [32]
CA_CH15_HighD	"	"	"	59%	"
CA_CH15_HalfD	"	"	"	30%	"
CA_CH15_woD	"	"	"	0%	"
HE_VW18_wD	Heating experiments (TD-AMS)	Smog chamber	Dry	15%	Isaacman-VanWertz, et al. [34]
HE_VW18_woD	"	"	"	0%	"
HE_SA16_wD	Heating experiments (TD-AMS)	Smog chamber	15–20%	8%	Saha and Grieshop [27]
HE_SA16_woD	"	"	"	0%	"

[a]Same as above. Abbreviations: PAM, potential aerosol mass; ESI, electrospray ionization; LC-TOF-MS, liquid chromatograph/time-of-flight-mass spectrometer; TD, thermodenuder; AMS, aerosol mass spectrometer; CIMS, chemical ionization mass spectrometer.

Table 3. Fitted parameters k_f, k_r, and D_b determined on the basis of formation and dilution experiments for the case of the CA-SA18-STD (Table 2). Estimated average parameters over 20 iterations are shown with one standard deviation.

Exp, #	Precursor	RH	$\log_{10}(k_f\ [s^{-1}])$	$\log_{10}(k_r\ [s^{-1}])$	$\log_{10}(D_b\ [m^2\ s^{-1}])$
1	α-pinene	<1%	–2.74 ± 0.07	–5.85 ± 1.45	–17.83 ± 0.05
2	α-pinene	<1%	–2.81 ± 0.09	–5.08 ± 0.18	–17.86 ± 0.01
3	α-pinene	<1%	–2.76 ± 0.07	–5.32 ± 1.25	–17.98 ± 0.06
4	α-pinene	40%	–2.88 ± 0.31	–3.97 ± 0.36	–15.41 ± 1.56
5	α-pinene	40%	–2.92 ± 0.06	–3.98 ± 0.08	–13.30 ± 0.83
6	α-pinene	40%	–2.74 ± 0.21	–3.90 ± 0.31	–15.14 ± 1.76
7	1,3,5-TMB	<1%	–2.81 ± 0.09	–8.30 ± 1.94	–18.13 ± 0.18
8	1,3,5-TMB	<1%	–2.72 ± 0.08	–6.26 ± 1.90	–18.06 ± 0.14
9	1,3,5-TMB	<1%	–2.73 ± 0.08	–6.44 ± 1.85	–18.13 ± 0.07
10	1,3,5-TMB	<1%	–2.52 ± 0.25	–3.70 ± 0.35	–18.62 ± 0.12

Abbreviations: RH: relative humidity, TMB: trimethylbenzene.

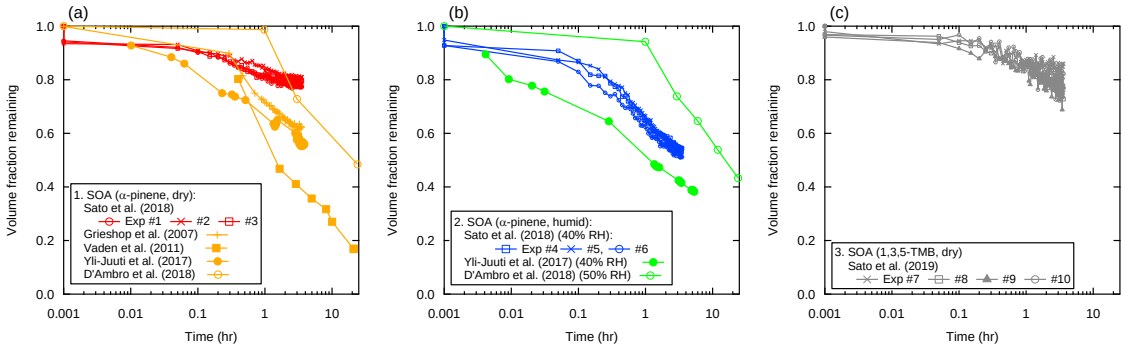

938

939 Figure 1. Measured volume fraction remaining of SOA from (a) α-pinene under dry conditions,
940 (b) α-pinene under humid conditions, and (c) 1,3,5-TMB under dry conditions after dilution.
941 Experimental results of Sato, et al. [33, 37] and other previous studies [23, 25, 55, 56] are shown (Table S3
942 of the SI).

943

944

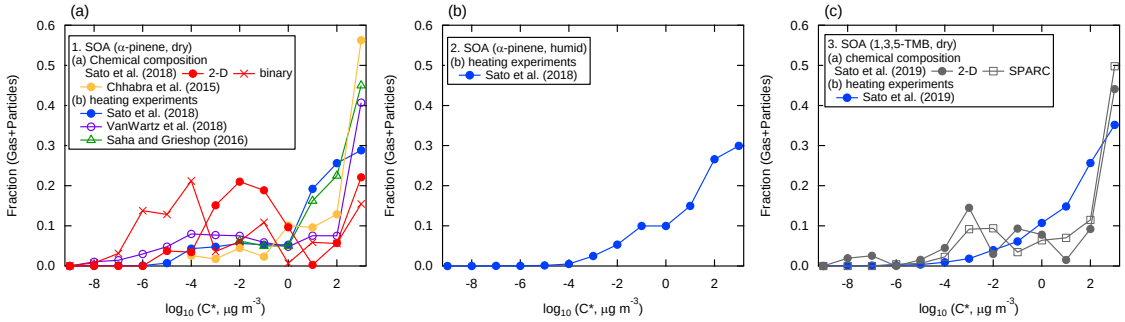

945

946 Figure 2. C^* distributions of SOA from (a) α-pinene under dry conditions, (b) α-pinene under
947 humid conditions, and (c) 1,3,5-TMB under dry conditions. Data estimated with a molecular
948 corridor approach of the both 1-D function (binary method) and 2-D function (2-D and SPARC
949 methods) are shown, and the details of these methods are described in Section 2.1. C^*
950 distributions estimated in the previous studies (Table 2) are also shown.

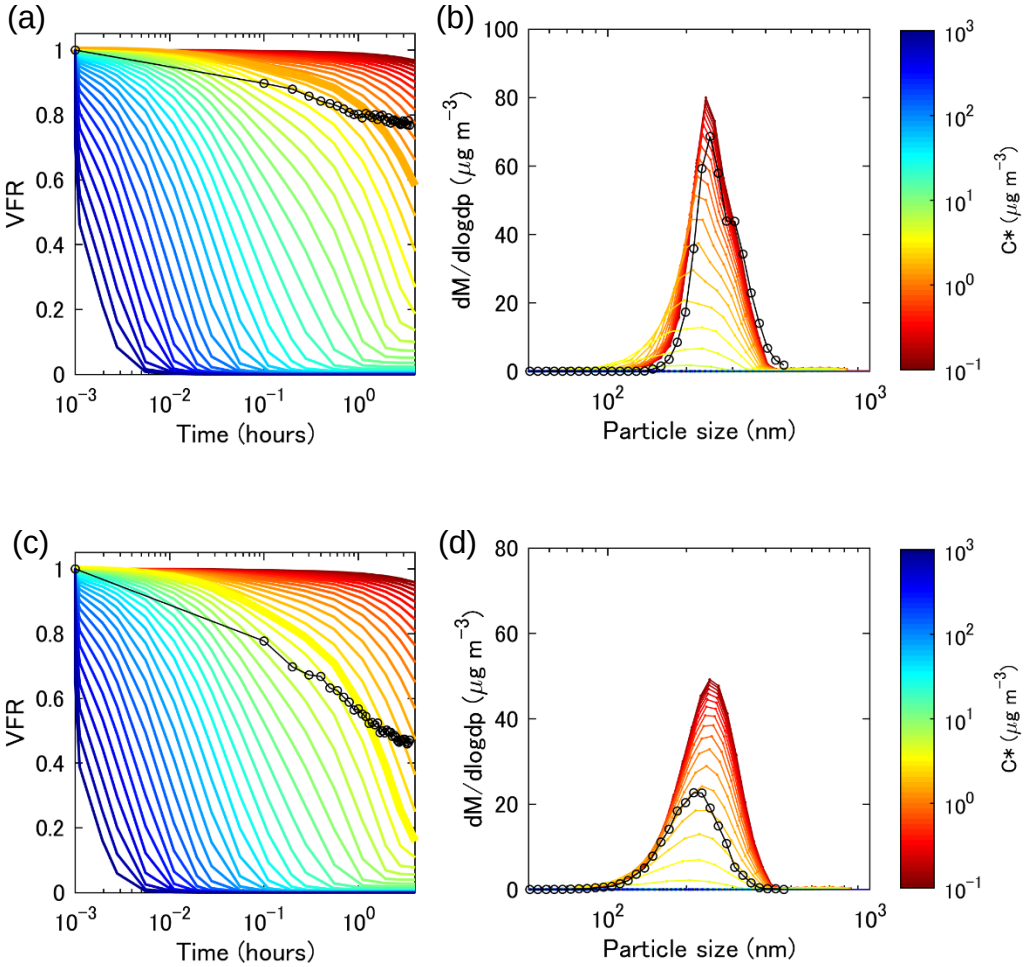

Figure 3. Volume fraction remaining (VFR) during dilution experiments (a and c) and mass size distributions ($dM/d\log D_p$) after 2 h from dilution (b and d) under dry (a and b, experiment #1) and humid (c and d, experiment #6) conditions. Black lines indicate observational results, and colored lines indicate results of simulation with different C^* compounds. Simulations results with the lowest RMSE are shown by thick lines. Simulations were conducted without consideration of dimer formation and bulk diffusion.

961

962

963

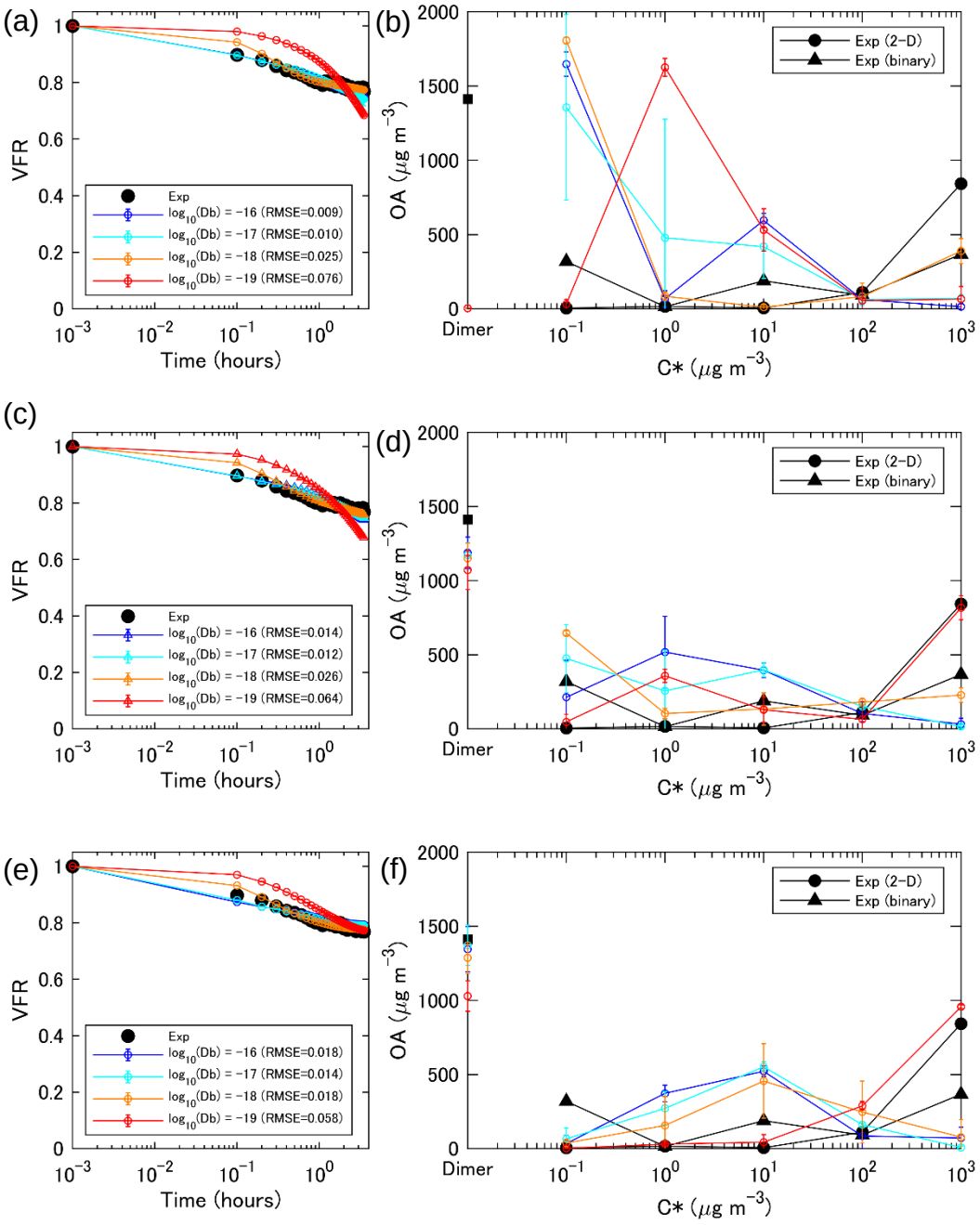

964 Figure 4. (left) Volume fraction remaining (VFR) during a dilution experiment and (right)
965 simulated C* distributions after a formation experiment under dry conditions (experiment #1). (a
966 and b) Dimer formation rates (k_f) were 10^{-6} s^{-1} and dimer dissociation rates (k_r) were 10^{-6} s^{-1}, (c
967 and d) $k_f = 10^{-3}$ s^{-1} and $k_r = 10^{-4}$ s^{-1}, (e and f) $k_f = 10^{-3}$ s^{-1} and $k_r = 10^{-6}$ s^{-1}. Observational results
968 are shown in black circles or triangles (by the parameterization of the 2-D and binary methods,
969 respectively, as explained in Section 2.1) and simulation results are shown in each color with

different D_b. Average and standard deviation of 20 simulations in each setup are shown. For the left figures, lines for $\log_{10}(D_b) = -16$ sometime overlap with the results for $\log_{10}(D_b) = -17$

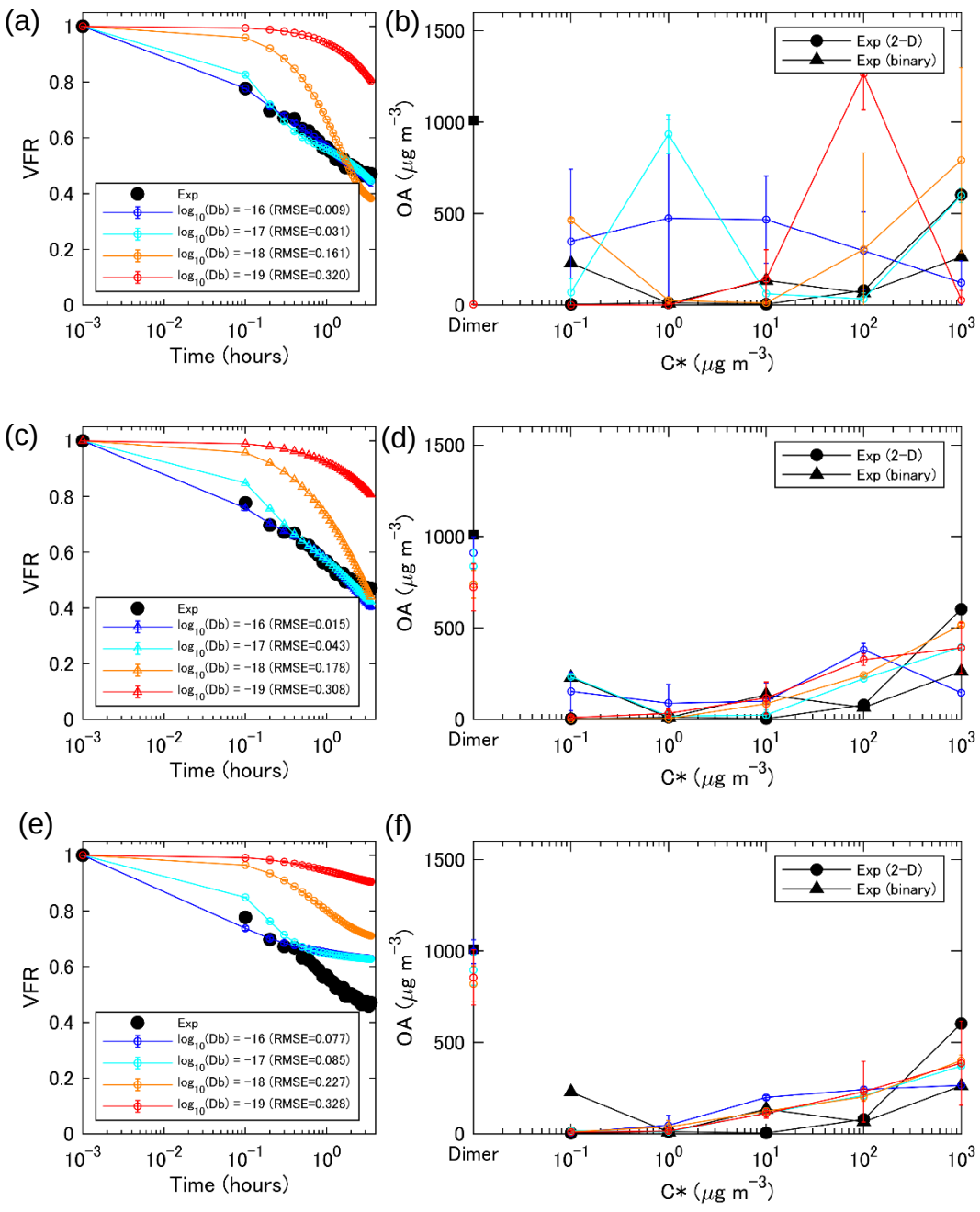

Figure 5. Same with Figure 4, but for an experiment under humid conditions (experiment #6).

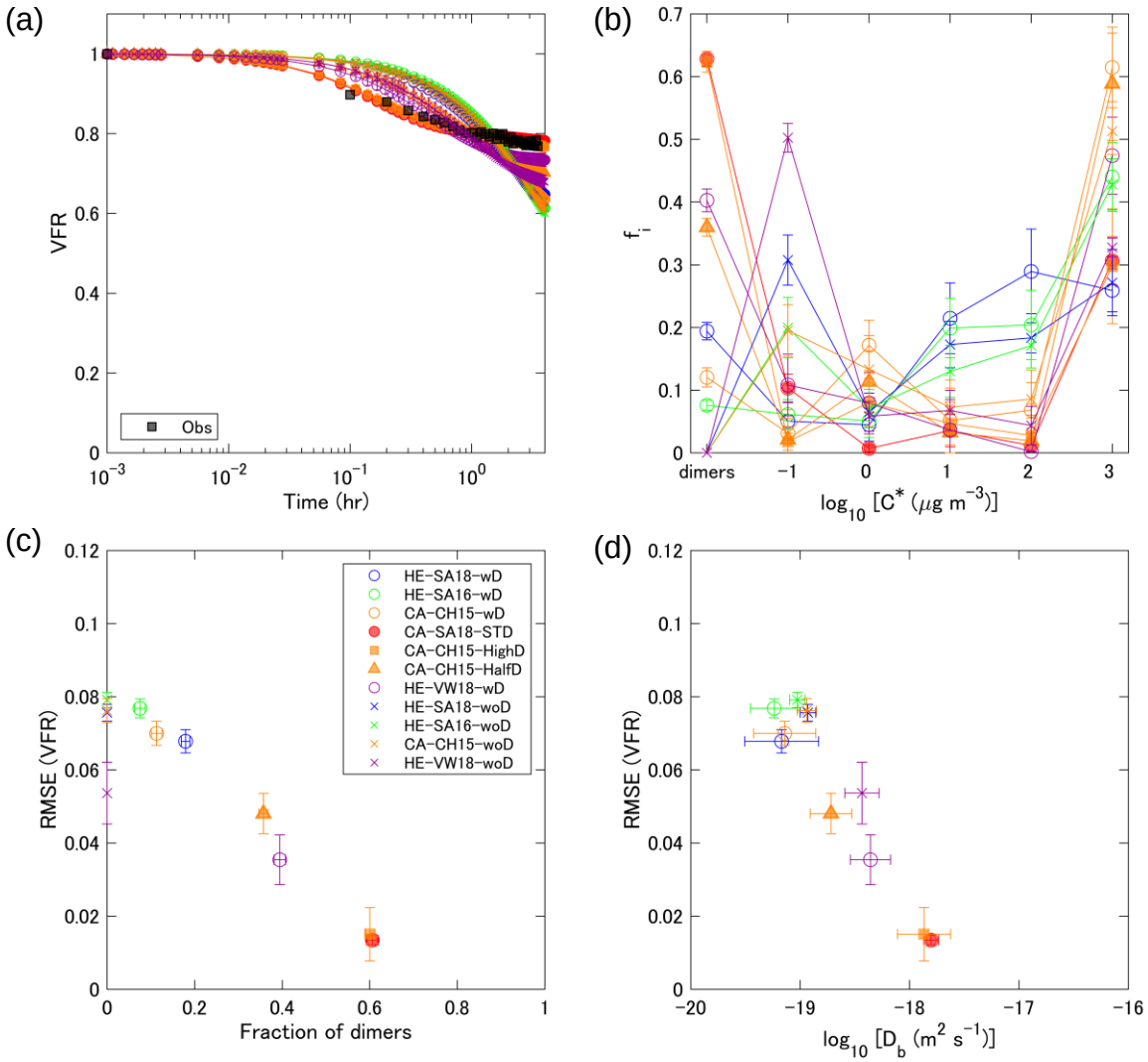

Figure 6. (a) Volume fraction remaining (VFR) during the dilution experiments for α-pinene SOA, as constrained by using C^* distributions obtained from the literature (Table 2). (b) C^* distributions of SOA (f_i) just before dilution. Relationship between root mean square error (RMSE) of the measured and simulated VFR and (c) the dimer fractions after the formation experiment or (d) diffusion coefficient (D_b). Error bars indicate one standard deviation of 20 iterative calculations in individual cases.

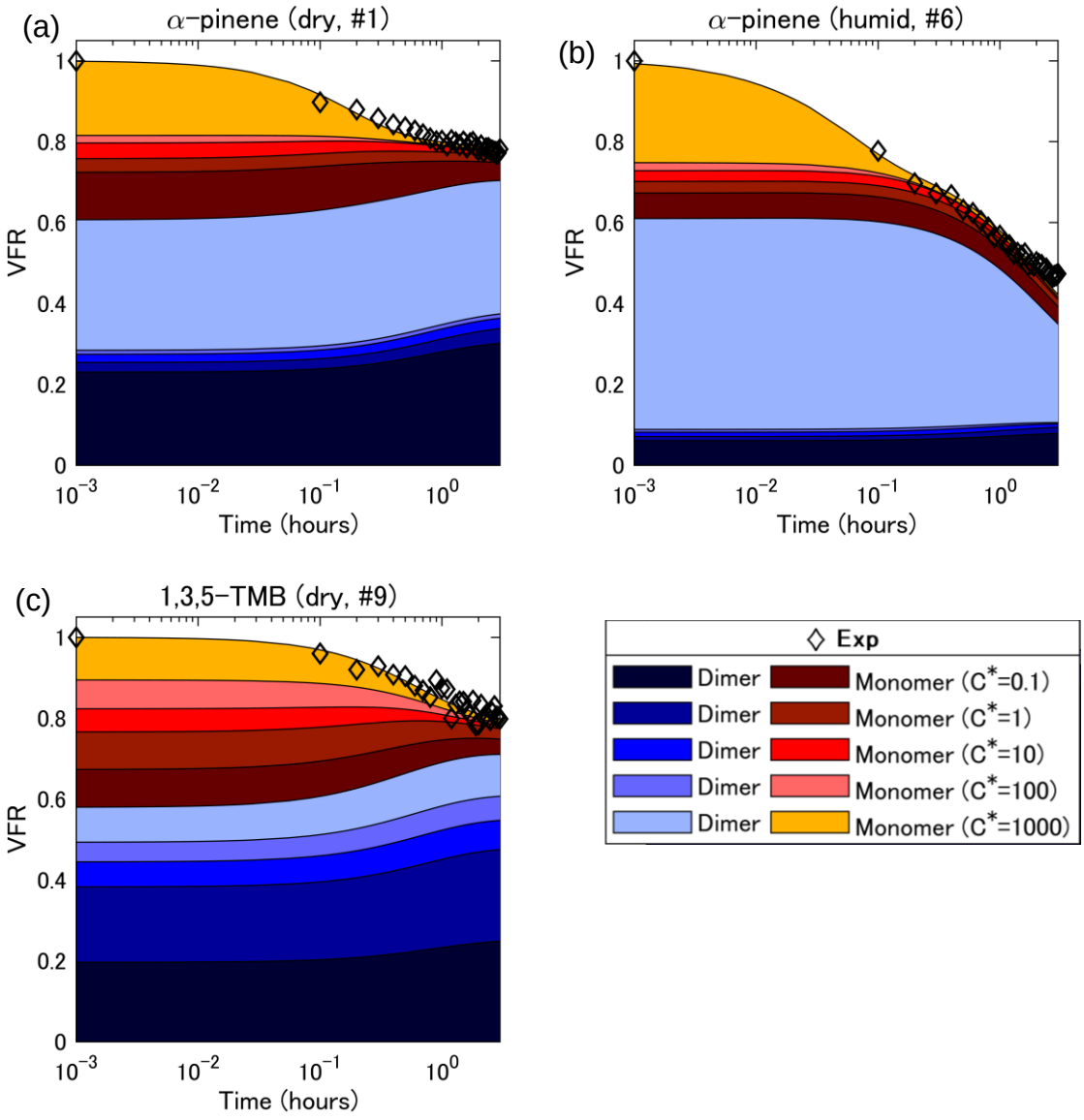

Figure 7. Volume fraction remaining (VFR) during dilution experiments for α-pinene SOA under dry (a, experiment #1) and humid (b, experiment #6) conditions or 1,3,5-TMB SOA under dry conditions (c, experiment #9). Each color indicates the contribution of monomer or dimer compounds with a saturation concentration (C^*) range from 0.1 to 1000 μg m^{-3}.

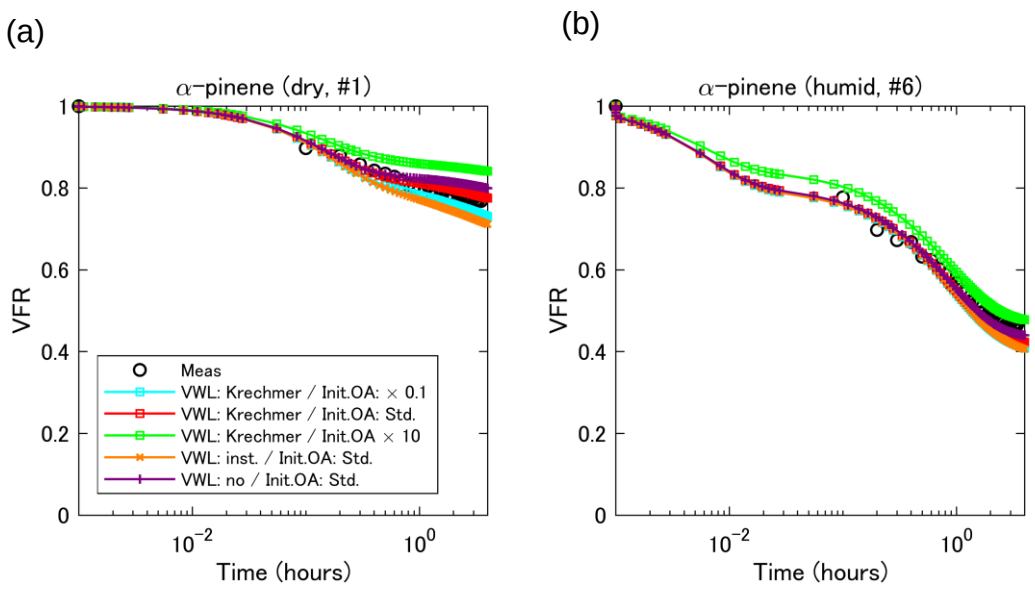

Figure 8. Volume fraction remaining (VFR) during dilution experiments under dry (a, experiment #2) and humid (b, experiment #6) conditions. Vapor wall loss was calculated with the methodology of Krechmer, et al. [46] (open circles) and with an assumption of instantaneous deposition (crosses).

1007 **TOC Art**

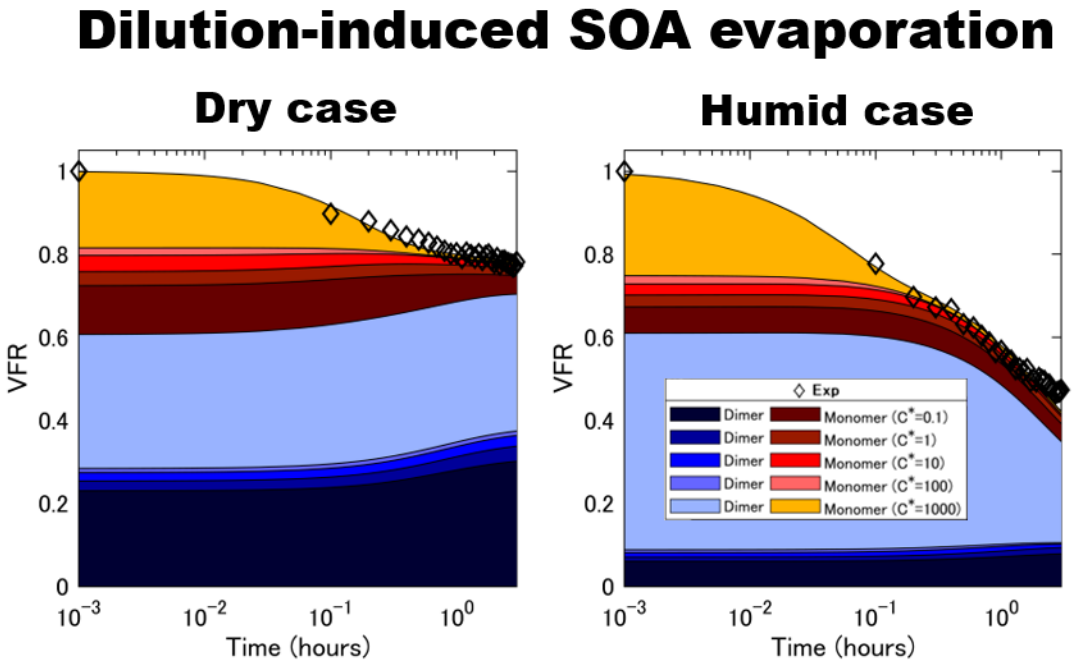

1008